JGR Atmospheres

RESEARCH ARTICLE
10.1029/2025JD043897

Photoelectric Effect in Air Explains Lightning Initiation and Terrestrial Gamma Ray Flashes

Victor P. Pasko[1], Sebastien Celestin[2], Anne Bourdon[3], Reza Janalizadeh[4], Zaid Pervez[1], Jaroslav Jansky[5], and Pierre Gourbin[6]

[1]School of Electrical Engineering and Computer Science, Penn State University, University Park, PA, USA, [2]Laboratory of Physics and Chemistry of the Environment and Space (LPC2E), OSUC, University of Orleans, CNRS, Orleans, France, [3]Laboratory of Plasma Physics (LPP), CNRS, Sorbonne Université, École Polytechnique, Institut Polytechnique de Paris, Palaiseau, France, [4]Space Weather Laboratory, NASA Goddard Space Flight Center, Greenbelt, MD, USA, [5]Department of Physics, Faculty of Electrical Engineering and Communication, Brno University of Technology, Brno, Czech Republic, [6]Department of Space Research and Technology (DTU Space), Technical University of Denmark, Kongens Lyngby, Denmark

Key Points:

- Photoelectric feedback discharges initiate lightning with no constrains on densities or physical origin of seed runaway electrons
- Photoelectric feedback discharges are a unified mechanism for production of initial breakdown pulses (IBPs), narrow bipolar events (NBEs), energetic in cloud pulses (EIPs), and terrestrial gamma ray flashes (TGFs)
- Similarity laws explain observed variability of IBPs, NBEs, EIPs, and TGFs produced at different altitudes in the Earth's atmosphere

Correspondence to:
V. P. Pasko,
vpasko@psu.edu

Citation:
Pasko, V. P., Celestin, S., Bourdon, A., Janalizadeh, R., Pervez, Z., Jansky, J., & Gourbin, P. (2025). Photoelectric effect in air explains lightning initiation and terrestrial gamma ray flashes. *Journal of Geophysical Research: Atmospheres*, *130*, e2025JD043897. https://doi.org/10.1029/2025JD043897

Received 17 MAR 2025
Accepted 22 JUN 2025

Abstract Terrestrial gamma ray flashes (TGFs) are high-energy photon bursts that have been linked to short bursts of electromagnetic radiation associated with lightning activity. The most puzzling unexplained aspect of these events is that gamma rays originate from very compact regions of space while the source regions often seem to be optically dim and radio silent when compared to processes in ordinary lightning discharges. In this work, we report a mechanism that allows precise quantitative explanation of these peculiar features of TGFs and their relationships to the observed waveform characteristics of associated radio emissions. The mechanism represents an extension of earlier ideas on feedback processes in growth of relativistic runaway electron avalanches (Dwyer, 2003, https://doi.org/10.1029/2003GL017781), and is based on a recent demonstration of the dominant role of the photoelectric feedback on compact spatial scales (Pasko, Celestin, et al., 2023, https://doi.org/10.1029/2022GL102710). Since discussed events often occur in isolation or precede formation of lightning discharges, the reported findings propose a straightforward solution for the long-standing problem of lightning initiation.

Plain Language Summary We provide explanation of spectacular naturally occurring bursts of X-rays and accompanying radio emissions that are observed in association with lightning activity in the Earth's atmosphere. These burst events are commonly referred to as terrestrial gamma ray flashes (TGFs). The core physical process leading to these events is avalanche multiplication of relativistic electrons accelerated by force exerted by electric field. In geophysical context, the electric field of sufficient magnitude and spatial extent for supporting these avalanches is generated either as an ambient field due to thundercloud electrification or produced in streamer zones of lightning leaders. These electrons radiate energetic photons (X-rays) as they scatter by nuclei of nitrogen and oxygen atoms in air. These X-rays are radiated in all directions and some fraction is radiated in opposite direction of electron motion. These particular X-rays lead to seeding of new relativistic seed electrons due to the photoelectric effect and thus strong amplification of the original avalanche. It has been established recently that these feedback effects occur on very small spatial scales, and in this work, we report the first fully time-dependent simulations of related dynamics, similarity analysis allowing better understanding of characteristics of events observed at different altitudes, and quantitative comparisons with observations.

1. Introduction

When measured at a close range, lightning initiation is often associated with a short ∼1 μs, low intensity, very high frequency (VHF) radiation pulse, and a weak quasi-static electric field change corresponding to electric dipole moment QL on the order of only ∼0.01 C km (Chapman et al., 2017; Marshall et al., 2014, 2019). Lightning initiation can be associated with much stronger VHF pulses with durations ∼10 μs that are accompanied by distinct wide band low frequency (LF) waveforms with very sharp rise times (1–2 μs) and dipole moment changes as high as QL ∼0.3 C km (Rison et al., 2016). These events are referred to as narrow bipolar events (NBEs). The sources of NBEs are also the strongest naturally occurring sources of terrestrial VHF radiation, yet they are light-deficient and often even optically undetectable compared to ordinary lightning discharges (Jacobson et al., 2013).

The sources of these events are compact (on the order of 100 m) and are referred to as compact intracloud discharges (CIDs) (Nag et al., 2010). It is recognized that these pulses are produced with highly variable magnitudes and many exist with much smaller magnitudes as well (Rison et al., 2016). Chapman et al. (2017) noted that weak NBE type events initiate some lightning flashes, but many events in the data set they studied (41 out of 71) had no detectable initiation pulse. NBE pulses are distinguished from other electromagnetic signatures produced by lightning due to their intensities and extremely short rise and fall times, and it has been known that these events, that can also occur in isolation (i.e., do not necessarily lead to lightning initiation), are very common and span over more than two orders of magnitude when presented on logarithmic (dB) scale (e.g., Smith et al., 2002, Figure 14, and references therein). Longer lasting pulses have also been observed with typical durations on the order of ~50–100 μs. These can be produced during initial breakdown activity before the formation of lightning leaders and usually are referred to as initial breakdown pulses (IBPs) (Marshall et al., 2013; Stolzenburg et al., 2013, 2016). More intense (in terms of inferred peak currents reported by lightning detection networks) versions of these pulses, that are likely associated with stepping of already formed negative leaders, are referred to as energetic in cloud pulses (EIPs) (Lyu et al., 2015, 2016; Ostgaard et al., 2021; Tilles et al., 2020). The electric dipole moments for these events are on the order of $QL \sim 10$ C km (Lyu et al., 2015; Marshall et al., 2013; Ostgaard et al., 2021; Stolzenburg et al., 2013, 2016; Tilles et al., 2020). These events have been associated with bursts of high-energy photons referred to as terrestrial gamma ray flashes (TGFs) (Lyu et al., 2016; Ostgaard et al., 2021) that are discussed in more detail in the next section. The EIPs are now considered as a robust identifier of TGFs (Lyu et al., 2016, 2024; Pu et al., 2019; Tilles et al., 2020). However, as was pointed in Pu et al. (2019) and as we further emphasize in the next section with review of more recent data, there are many TGFs that are not associated with EIPs. Marshall et al. (2013) and Stolzenburg et al. (2013, 2016) did not have correlations of their reported events with TGFs. However, they suggested that phenomenology of their events agreed with what was known at that time about lightning initiating discharges leading to TGFs. In this work, we provide interpretation of fine subpulses embedded in IBP field changes reported in Marshall et al. (2013) and Stolzenburg et al. (2013, 2016) in terms of discrete relativistic electron avalanches and therefore provide supporting evidence for their hypothesis.

The feedback effects in development of relativistic electron runaway avalanches have been first introduced in Dwyer (2003). An explosive growth of the avalanche occurs when positrons and X-rays are launched backward to the origin of the avalanche and provide additional seeding and replenishment of the avalanche (Dwyer, 2003). This process has a direct analogy with photoionization feedback in conventional discharges in air when electron avalanches self-replicate themselves as ultraviolet photons emitted by N_2, which is excited due to electron impact, travel back to the avalanche initiation/source region, and ionize O_2 upon absorption to feed new avalanches (Naidis, 2005). In the relativistic case, there are three principal pathways for the feedback process and each can be characterized by corresponding energy and ambient air pressure-dependent spatial scale: photoelectric absorption l_{pe}, Compton scattering l_c, and pair production l_{pp} (Pasko, Celestin, et al., 2023, Figure 2c). Bremsstrahlung photons traveling from the avalanche toward the seeding region participate in the production of runaway electrons through photoelectric absorption and Compton scattering. These processes are usually referred to as X-ray feedback (Dwyer, 2003). Photoelectric effect is the most efficient feedback process on small time and spatial scales as it has the shortest range $l_{pe} < l_c < l_{pp}$ and involves direct flight of bremsstrahlung photons from the avalanche toward the seeding region, not requiring additional scattering interactions involved in the Compton scattering and pair production feedback channels (Pasko, Celestin, et al., 2023). Using the physical analogy with photoionization feedback in conventional discharges, we refer to the discharges reported in this paper as photoelectric feedback discharges. A recent study indicates that the photoelectric feedback process plays a dominant role under controlled conditions in high voltage experiments, in particular, explaining how electrons with anomalously high energies (exceeding those dictated by the applied voltage by a factor of 3) are produced (Pasko et al., 2024). The modeling methodology employed in the present work is based on a differential formulation developed for photoionization feedback problems (Jansky & Pasko, 2020; Jansky et al., 2025; Pasko, Janalizadeh, & Jansky, 2023).

The purpose of this paper is to demonstrate that relativistic runaway electron avalanches can very quickly multiply due to the photoelectric feedback process and to provide a unified explanation of short time and compact spatial scales for the types of discharges discussed above, including those involved in lightning initiation. The photoelectric feedback discharges directly correspond to the process referred to as fast positive breakdown in the existing literature (Rison et al., 2016) that we discuss in detail below. Our findings are in agreement with the

recent analysis of Huang et al. (2021) indicating that a short and not always easily detectable fast positive breakdown event (Rison et al., 2016) with various magnitudes is commonly present as a lightning initiation event. We also demonstrate how, depending on the vigor of growth, spatial scale and magnitude of the thundercloud electric field, the photoelectric feedback discharges can lead to fast positive breakdown with or without strong VHF producing streamer activity.

2. Phenomenology of TGFs and Related Radio and Optical Emissions

Spectacular naturally occurring bursts of X-rays with tens of mega electron volt energies are observed in association with lightning activity in the Earth's atmosphere. These events were first discovered in 1994 by NASA's Compton Gamma Ray Observatory (Fishman et al., 1994) and are commonly referred to as terrestrial gamma ray flashes (TGFs). Although since then many other orbital observatories captured these high-energy events (Briggs et al., 2011; Marisaldi et al., 2010; Neubert et al., 2020; Smith et al., 2005) and these events have been clearly linked to very intense but short (approximately 10–50 microseconds) bursts of electromagnetic radiation (Lyu et al., 2016; Ostgaard et al., 2021), the physical nature of these events remains unclear. Lu et al. (2010) provided evidence of association of TGF sources with initial development of compact intracloud lightning flash when an inferred upward propagating leader extended in length from 1.5 to 2 km in a form of five discrete fast discharges. As was noted in the introduction, EIP pulses are currently considered as a reliable radio signature of a subset of TGFs. The EIP pulses can be preceded by several milliseconds by flash initiating NBE events, and in one observation, the EIP sferic evolved independently from streamer activity producing VHF emissions, leading the authors to suggest that the EIP sferic was produced by relativistic discharge currents (Tilles et al., 2020). In the same event, the inferred relativistic currents during the main sferic pulse initiated a strong NBE-like event comparable in VHF power to the highest-power NBEs (Tilles et al., 2020), providing an example of a hybrid event in which the relativistic discharge process evolved with and without VHF producing streamer activity.

Stanley et al. (2006) reported a TGF event that likely occurred at or near-time of flash initiation. Two NBE events reported in Shao et al. (2010) and Stanley et al. (2006) were delayed by 3.3 and 2.9 ms, respectively, with respect to TGFs observed from the orbit, leading these authors to conclude that NBE and TGF events are not related. Zhang et al. (2021) reported nine TGFs that preceded the occurrence of NBEs by a minimum of 60 μs up to 13.5 ms, and no other fast leader discharge was found within 20 ms before the TGF. The analyses in Zhang et al. (2021) show that the NBE-preceding-TGFs bear harder energy spectrum with larger proportion of high-energy photons than EIP-related TGFs produced in association with lightning leaders. In the context of present work, the authors made an important suggestion that the gamma ray production by the thunderstorm electric field could make conditions favorable for the occurrence of NBEs. Ostgaard et al. (2021) provides evidence indicating simultaneity of EIP sferics and TGFs, likely produced during leader stepping. There are many TGFs observed from orbit, especially longer duration ones, with no detectable sferics (Bjorge-Engeland et al., 2022). This once again reiterates the point stated already in the introduction section that there are many TGFs that are not associated with EIPs (Pu et al., 2019). Pu et al. (2020) reported satellite observation of a TGF produced during the initial leader development of a cloud to ground lightning flash. The TGF coincided in time with ≃120 μs LF/VLF pulse and was generated 3 ms after the initiation of a downward negative leader and 3 ms preceding a −146 kA peak current cloud to ground stroke (Pu et al., 2020). This scenario is consistent with TGF production during one of the steps of propagating the stepped leader (Abbasi et al., 2023).

The recent TGF observations obtained at a close range from either high-altitude aircraft (Bjorge-Engeland et al., 2024; Marisaldi et al., 2024; Ostgaard et al., 2024) or ground (Abbasi et al., 2018, 2023, 2024; Belz et al., 2020) are of special interest for understanding of their phenomenology, and we discuss these in the next paragraphs.

There is a population of TGFs that are not detectable from the orbit, and these events may or may not be associated with sferics detectable by lightning location networks (Bjorge-Engeland, 2024; Bjorge-Engeland et al., 2024). Space instruments have observed TGFs with a total number of photons emitted at the source down to $\sim 10^{16}$–10^{17}, and two to five orders of magnitude lower values (10^{12}–10^{15}) have been documented in recently reported high-altitude aircraft observations (Bjorge-Engeland et al., 2024).

The high-altitude aircraft observations of Ostgaard et al. (2024) also show for the first time the sequence of events produced by the growth of electric field in thundercloud electrical environment that leads to a sequence of flashes

of gamma rays with no detectable radio or optical emissions. The observed time sequences of gamma ray pulses resemble those in the paper originally reporting the discovery of TGFs (Fishman et al., 1994). The authors term these as flickering gamma ray flashes (FGFs) (Ostgaard et al., 2024). The radio silence and optical darkness of these events are truly remarkable, and the sequence of FGFs is followed by an abrupt electric field change and a classic NBE event that initiates an episode with continuous VHF electromagnetic emissions, that is a familiar characteristic of propagating lightning leaders. The NBE event is delayed with respect to last detectable gamma ray pulse by several milliseconds (Ostgaard et al., 2024). These millisecond scale delays are consistent with earlier reports in Shao et al. (2010), Stanley et al. (2006), and Zhang et al. (2021) reviewed above. Ostgaard et al. (2024) demonstrate for the first time that this sequence of events is repeatable, and that the documented birth of lightning involves and is likely facilitated by the high-energy electrons responsible for the observed gamma ray flashes that are apparently present in the same physical space where lightning-initiating NBE event is produced just several milliseconds later. The work we report in this paper advances a hypothesis that the NBE event coincides with the last photoelectric feedback pulse when growing ambient field in thundercloud satisfies conditions for streamer propagation and growth. Streamers are effectively seeded by the abundance of electrons produced by photoelectric feedback discharge and the process culminates in the fast field discharge by streamers that produces sharp CID current waveform leading to emission of the NBE sferic. One of the important contributions of the present work is that we demonstrate that sequence of weak electric field changes (Chapman et al., 2017; Marshall et al., 2014, 2019) and pulsations reported in Fishman et al. (1994) and Ostgaard et al. (2024) can be quantitatively explained using the same photoelectric feedback principles that we formulate in this work.

Abbasi et al. (2018) report ground-based observations of TGFs by the telescope array surface detector in Utah, USA, associated with downward-propagating negative leaders. The authors noted that the durations of the individual TGF pulses were $\leq$10 μs, and the overall sequence of events was consistent with one or two particularly energetic leader steps that were confined to the first 1–2 ms of these discharges (Abbasi et al., 2018). We note that the phenomenology of these events is consistent with that in which X-ray emissions from stepping lightning leaders were originally discovered (Dwyer et al., 2005; Moore et al., 2001). Abbasi et al. (2018) made a significant discovery that energies of these photons extend into the multi-MeV range and estimated a total number of gamma ray photons in these events to be on the order of 10^{12}–10^{14}. Abbasi et al. (2018) note that these events are essentially the same events as those observed by satellites, but the ground-based observations are more representative of the temporal source activity and are also more sensitive than satellite observations, which detect only the most powerful TGF flashes. The detailed Monte Carlo simulations of photon transport indicate that if pulses of duration shorter than 10 μs with tens of microseconds separation occur in the production of TGFs, they should be observable from space, given instrumentation with sufficient time resolution (Berge & Celestin, 2019). It is noted that the TGF-producing storms reported in these studies had low flashing rates (typically 1–2 min between flashes) apparently allowing the electrification to build up to large values (Belz et al., 2020). The most recent studies indicate photon counts up to 8×10^{14} in reported TGF events (Abbasi et al., 2024). We note that these are lower counts in overall distribution of published TGFs spanning nine orders of magnitude (Abbasi et al., 2018, 2024; Chaffin et al., 2024; Lindanger et al., 2021).

Belz et al. (2020) reported association of TGFs produced during IBPs with subpulses remarkably resembling those reported in Marshall et al. (2013) and Stolzenburg et al. (2013, 2016) (discussed in the introduction section of this paper). Specifically, the authors state that TGFs are often initiated at the time of characteristic "sub-pulses" that occur during large-amplitude, "classic" IBP sferics. They explain these as produced by spark-like transient conducting events and write (Belz et al., 2020): "That the events are spark-like is indicated by the pointed, cusp-like nature of their sferics, evidence of a sudden current onset and rapid turnoff, and also by the sub-pulses repeating several times as the IBP progresses. It should be noted that the final peak of the overall IBP sferic is also cusp-like, indicating that it too is produced by a spark-like sub-pulse." The authors also provide a convincing evidence (please refer to their Figures 3 and 6, and also Figure 4 in Marshall et al. (2013)) of remarkable similarities between IBPs with these subpulse structures initiating intracloud (IC) discharges and negative cloud to ground (−CG) discharges. As already noted in the introduction section, in this work, we provide interpretation of these fine subpulses in terms of discrete bursts of relativistic electron avalanches. These fine subpulses embedded in IBP, NBE, and EIP waveforms can be seen in many reported data sets (Chen et al., 2024; Karunarathne et al., 2021; Liu et al., 2022; Nag & Rakov, 2010; Pu et al., 2019; Rison et al., 2016). A careful inspection of data shown in Belz et al. (2020) provides evidence of weak fast positive breakdown events in some of the reported events in agreement with ideas of Huang et al. (2021) discussed in the introduction section. Belz et al. (2020) also

point to significant differences in durations of the TGFs, being ≃5–10 μs for the downward –CG TGFs, versus ≃20–200 μs for the upward, IC-generated TGFs. They also note that IC subpulses had amplitudes of ≃10–20 V/m, compared to ≃5–10 V/m for −CGs (Belz et al., 2020). They also indicate that IC IBPs tend to have longer durations than those of –CGs, lasting ≃70 μs for the IC IBP versus ≃35 μs for the −CG IBP (Belz et al., 2020). Similar trends are noted in many other publications including those cited above (Chapman et al., 2017; Marshall et al., 2014, 2019) with observed scaling apparently not being understood yet (see discussion in Chapman et al. (2017)). In our study, we provide detailed analysis of photoelectric feedback discharges in scaled form and explain variability of various physical quantities, including the factor of two differences noted above, by variations in ambient air density at different altitudes in the Earth's atmosphere. Readers are referred to Figure 3 in da Silva and Pasko (2015) as a reference for general altitude structure of charges (including midlevel negative and upper-level positive augmented by lower positive and negative screening at the upper cloud boundary) in classical normally electrified midlatitude thunderstorms leading to initiation of different types of discharges. It should be noted that charge distributions shift upward by 4–5 km at higher latitudes in tropical thunderstorms due to the increase in height of tropopause with latitude (e.g., Williams et al., 2006).

High-speed video recordings of luminosity of IBP pulses that precede the conventional stepping leader development were reported in Stolzenburg et al. (2013, 2016). As was noted in the introduction section, the authors did not have associated TGF recordings. However, given our current knowledge reviewed above, these are the same IBPs that are now known to produce TGFs. Stolzenburg et al. (2013, 2016) report one to one alignment of optical pulses and weak NBE-like pulses forming IBP sequences discussed above. Stolzenburg et al. (2013) referred to these pulses as surges of initial leaders because in comparison with conventional stepped leaders, they were longer, brighter, more separated in time, unbranched, and relit rearward along the entire developing feature back to the initial point of the flash. We note that for these -CGs the electric field points upward, relativistic electrons would avalanche downward and the fast positive breakdown, that is discussed below in this paper, would propagate upward. The observations of Stolzenburg et al. (2013) may therefore be the first direct imaging of the fast positive breakdown. Stolzenburg et al. (2013) emphasize that an IB pulse is caused by a substantial current surge that is hundreds of meters long. Stolzenburg et al. (2013) also report another type of IB light that is characterized by a bright spot, typically appearing a few hundred meters across at maximum, with the luminosity of the spot increasing over two to three video frames (≃20 μs image interval), and then dimming over the next few frames. It has also been discovered that during the return stroke that followed, this initial region, in which IBP pulses are forming, behaves differently from the channel below, indicating it is less conductive (Stolzenburg et al., 2014). It should be emphasized that TGFs are produced during initial breakdown pulses (IBPs) in the first few milliseconds of the flash (Belz et al., 2020), and also several hundred microseconds later during propagation of the stepped leader when the leader was observable and video-recorded below the cloud base (Abbasi et al., 2023). The spectroscopic data available during time intervals when TGFs are produced during leader steps indicate that spectra is dominated by ionized and neutral atomic lines (including a 777.4-nm atomic oxygen line usually associated with hot thermalized leader or return stroke channels) before, during, and after the TGF event, with neutral atomic emissions enhanced during the TGF event (Kieu et al., 2024). The authors contrast these observations with orbital detections of optical emissions associated with TGFs. In published orbital records, the onset of TGFs precedes onset of 337.1 and 777.4 nm optical pulses when these are detectable (Bjorge-Engeland, 2024; Bjorge-Engeland et al., 2024; Ostgaard et al., 2021; Skeie et al., 2022). We note that passband 400–900 nm in Kieu et al. (2024) would not allow detection of a (0,0) 337.1-nm s positive band of molecular nitrogen N_2. However, it would allow detection of a strong (0,1) 427.8-nm band of the first negative band system of N_2^+, that would be a signature of strong nonthermal discharges (streamers). The 427.8 nm emission has not been detected in Kieu et al. (2024). Mezentsev et al. (2024) report orbital observations of a bright long duration TGF together with its associated optical recordings (including both blue 337.1 nm streamers, and red 777.4 nm leader emissions) showing clear temporal separation between the TGF and the optical pulse, with the optical pulse being clearly distinct and subsequent relative to the TGF.

Gurevich et al. (2006) considered NBEs as manifestation of relativistic runaway breakdown initiated by extensive atmospheric showers. The process was linked to lightning flash onset and gamma ray emissions, and modeled in a large (several km) domain without consideration of feedback processes discussed in present work. A joint action of large cosmic ray-extensive air showers with relativistic runaway electron avalanche multiplication was discussed in Dwyer and Uman (2014, Section 6.5, and references therein) as a possible mechanism of NBEs, and the related studies of Arabshahi et al. (2014) concluded that unrealistic thunderstorm properties are required to

explain measured properties of NBEs. Recently reported evidence indicates apparent ignition of lightning by cosmic-ray showers (Shao et al., 2025).

In Pasko, Celestin, et al. (2023), it was suggested that there are two principal photoelectric feedback scenarios when TGFs are produced: as lightning initiation event due to thundercloud electrification or as part of stepping progression of already initiated negative lightning leader. We demonstrate below that majority of experimental findings reviewed above can be understood from a common physics point of view. In particular, we require satisfaction of identical feedback conditions for the electrification and stepping scenarios, and demonstrate below that X-ray photon fluxes can be substantial even in cases when sferics may not be observable (the feedback discharge may not produce either LF/VLF spectral content or sufficient current moments for detection). We show how very weak sferics are produced by the photoelectric feedback discharges that have very short (microsecond scale) durations and comparable to those often seen as lightning initiation events. In our work, we also relate known and well-documented occurrences of strong NBE and EIP sferics and TGFs. The proposed modeling framework allows quantitative explanation of the vast majority of currently accumulated observations of these weak and strong events at different altitudes in the Earth's atmosphere from common physical perspective. The specifics include TGF fluences and durations, optical darkness, magnitudes of low and very low frequency (LF and VLF) IBP, NBE and EIP sferics, including characteristic fine pulsations often seen embedded in waveforms of these events, existence of weak IBP events that consist of a sequence of weak NBE-like pulses, presence or absence of strong VHF emissions, the peculiar observations of very fast (typically one tenths of the speed of light) spatial propagation features termed fast positive breakdown in the present literature, pulsing of TGFs, appearance of lightning initiating NBE event several milliseconds after several optically dark and radio silent TGF pulses, appearance of TGF pulses after the lightning initiating NBE event, and low fluence TGFs not observable from the orbit.

3. Model Formulation

The geometry of one-dimensional coordinate z dependent domain is depicted in Figure 1a. The relativistic runaway electrons avalanche from right to left in the discharge volume and emit the bremsstrahlung X-rays due to their interaction with air. The model has provision to initiate the runaway electron population with a seed density of one electron per m^3 placed at $t = 0$ and $z = d$, or continuous ambient source S_0 ($m^{-3}s^{-1}$) introduced in the entire domain. The relativistic runaway electrons also produce abundant quantities of low-energy secondary electrons, positive ions, and negative ions formed by quick two- and three-body electron attachment processes. All numerical implementation details that would allow readers to reproduce results of this work are included in Appendix A. The model representation of electric field E_a applied over distance d is created by two surface charge densities of equal magnitude but opposite polarity ρ_s^+ and ρ_s^- as depicted in Figure 1a. We use a scaling factor $\delta = n/n_0$, where n is altitude-dependent air number density and $n_0 = 2.688 \times 10^{25}$ m^{-3} is a reference value corresponding to standard atmospheric conditions at sea level in Earth's atmosphere. We refer to the scaled field E_0/δ as the reduced applied electric field required for the inception of self-sustained relativistic runaway discharges in air. This field is a function of the reduced physical dimension of space over which this electric field is applied, that is, $d\delta$, where d denotes the distance over which the electric field is applied. In the range $100 < d\delta < 160$ m, the E_0/δ distribution can be approximated as $E_0/\delta = 3.728 \times 10^2\ (d\delta)^{-0.697}$ kV cm^{-1}, where $d\delta$ is in units of meters. The full distribution is documented in Pasko, Celestin et al. (2023), included in Appendix A as Figure A1a, and discussed further in Figure 7. Figure A1a includes the abovementioned fit, and both Figures A1a and 7 provide reference value for the electric field in the streamer zone of negative lightning leader $E_{cr}^-/\delta = 12.5$ kV cm^{-1} discussed in Pasko, Celestin, et al. (2023). In fields with magnitudes comparable and exceeding E_{cr}^-/δ, negative streamers can propagate. The E_{cr}^-/δ field is greater than the corresponding field $E_{cr}^+/\delta = 4.4$ kV cm^{-1} for positive streamers. Therefore, the double-headed streamers can grow exponentially in applied fields exceeding E_{cr}^-/δ as they can self-consistently support simultaneous exponential growth of negative and positive charges in their respective heads. The exponential growth of the streamers can be characterized by corresponding time scale $\tau_s\delta$ that is a sensitive function of the applied electric field E_a/δ (Pervez et al., 2024b). All reported numerical results in this paper do not explicitly include space charge effects, VHF radiation, or optical emissions produced by streamers. Streamers are considered as a derivative of the photoelectric feedback process and their ability to contribute to space charge effects, produce VHF radiation, and blue optical emissions is acknowledged only qualitatively when results are discussed in context of existing observations. For the purposes

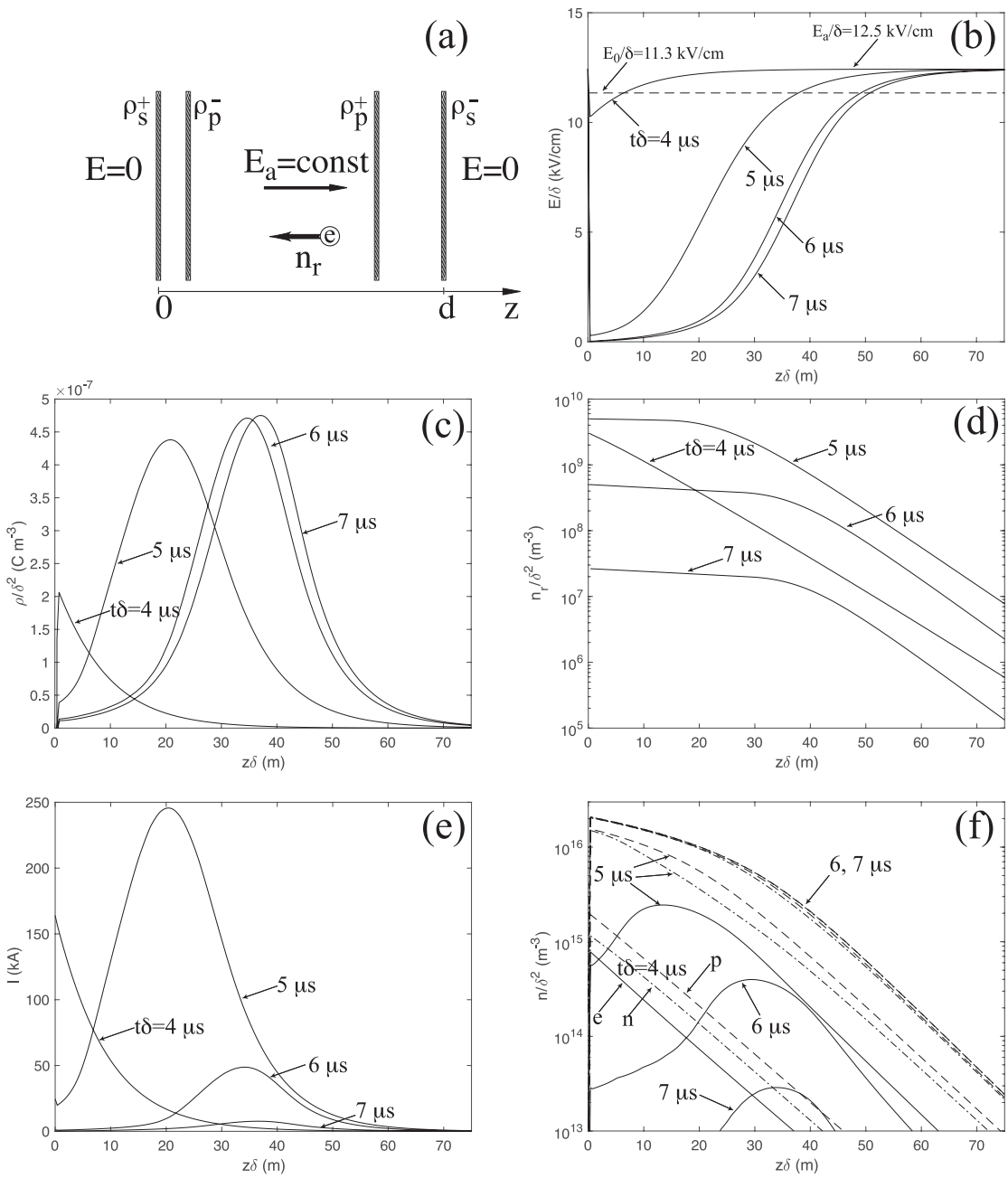

Figure 1. (a) Schematics of a one-dimensional simulation domain. (b) The reduced electric field E/δ. (c) The reduced charge density ρ/δ^2. (d) The reduced number density of runaway electrons n_r/δ^2. (e) The current I. (f) The reduced number densities n/δ^2 of electrons (e, solid line) and positive (p, dashed line) and negative (n, dashed-dotted line) ions. The quantities are shown as functions of reduced coordinate $z\delta$ at selected moments of reduced time $t\delta$ for the case of $d\delta = 150$ m, $E_a/\delta = 12.5$ kV/cm at altitude $h = 11$ km and assuming a continuous ambient source of runaway electrons S_0.

of discussion that follows in this paper, it is important to note that in applied fields, $E_a/\delta > E_{cr}^-/\delta$ streamers can grow with rates that are faster than the growth rate of relativistic runaway electron avalanches $\tau_r\delta \simeq l_r\delta/c$, where c is speed of light in free space and $l_r\delta$ is the corresponding applied field-dependent runaway electron multiplication length (Dwyer et al., 2012) (definition is included in Appendix A). Streamers require seed electrons for their initiation, and we suggest that the relativistic feedback discharges provide abundance of seed electrons that facilitate growth of streamers when $E_a/\delta > E_{cr}^-/\delta$ and $\tau_s\delta < \tau_r\delta$, and streamers can play a significant role in space charge dynamics and screening of the applied electric field. For applied fields $E_a/\delta \leq E_{cr}^-/\delta$, relativistic feedback discharges grow with no participation of streamers, that can be interpreted as $\tau_s\delta \gg \tau_r\delta$. We demonstrate below

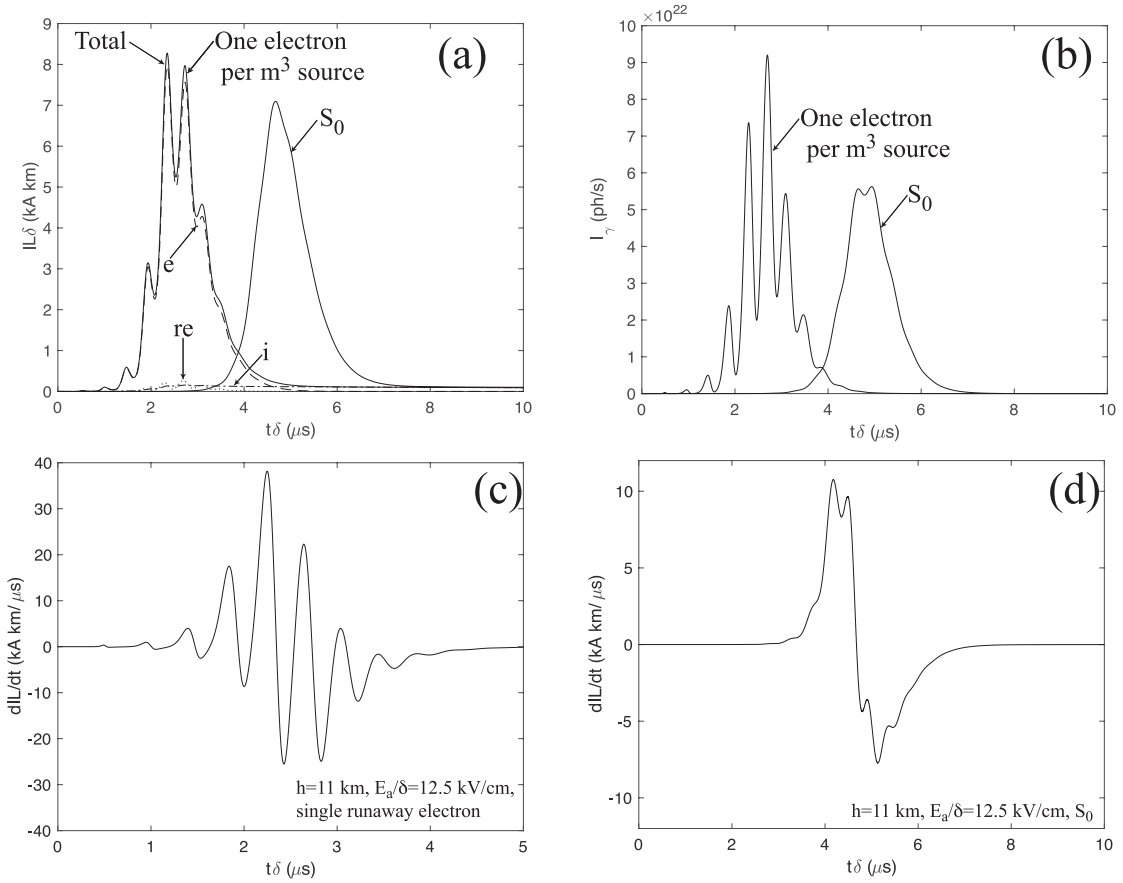

Figure 2. (a) The reduced current moment $IL\delta$, also illustrating relative contributions to the total current of electrons, e; relativistic electrons, re; and ions, i. (b) The emission intensity of gamma rays I_γ. Panels (c) and (d) show corresponding time derivatives $\frac{d}{dt}(IL)$ for cases shown in panels (a) and (b) (these do not scale with air pressure). The quantities are shown as functions of reduced time $t\delta$ for the case of $d\delta = 150$ m, $E_a/\delta = 12.5$ kV/cm at altitude $h = 11$ km, for the cases of one electron per m^3 excitation, and for the continuous ambient source of runaway electrons S_0 (see text).

that magnitude and vigor of growth of E_a/δ with respect to E_0/δ can produce both very strong and very weak discharges, with and without VHF emissions produced by streamers. Very broadly, one can associate examples of gamma ray glows and flickering gamma ray flashes (FGFs) observed in Eack and Beasley (2015), Eack et al. (1996), Marisaldi et al. (2024), and Ostgaard et al. (2024) with $E_a/\delta > E_0/\delta$ and $E_a/\delta \leq E_{cr}^-/\delta$, a TGF event observed in Ostgaard et al. (2021) with $E_a/\delta > E_0/\delta$ and $E_a/\delta > E_{cr}^-/\delta$, and a hybrid event observed in Tilles et al. (2020) with a situation when the driving field is $E_a/\delta > E_0/\delta$ and evolves from values $E_a/\delta < E_{cr}^-/\delta$ with no streamers and VHF emissions to $E_a/\delta > E_{cr}^-/\delta$ with streamer-induced VHF emissions during the event evolution. It should be noted that in real geophysical situation, the feedback conditions $E_a/\delta > E_0/\delta$ can be satisfied by either keeping the gap size $d\delta$ constant and increasing of E_a/δ in time (this corresponds to vertical motion in Figure A1a), or keeping E_a/δ constant and increasing of the gap size $d\delta$ in time (this corresponds to horizontal motion in Figure A1a), or by any complicated combination of these two. To simplify illustration of principal ideas of this work in all simulations presented in this paper, the simulation domain size is kept constant, and all effects are demonstrated by either applying E_a of different magnitudes (as a step function at $t = 0$), or increasing E_a as a function of time with different rates and different model-defined functional dependencies on time.

4. Results and Discussion

4.1. Properties of Photoelectric Feedback Discharges as a Function of Applied Field E_a

The step like application of the electric field in time discussed in this section is more readily applicable to cases when TGFs are produced by stepping of negative lightning leaders that would provide fast increase of the field above the relativistic feedback threshold in their negative streamer zones as discussed in Pasko, Celestin,

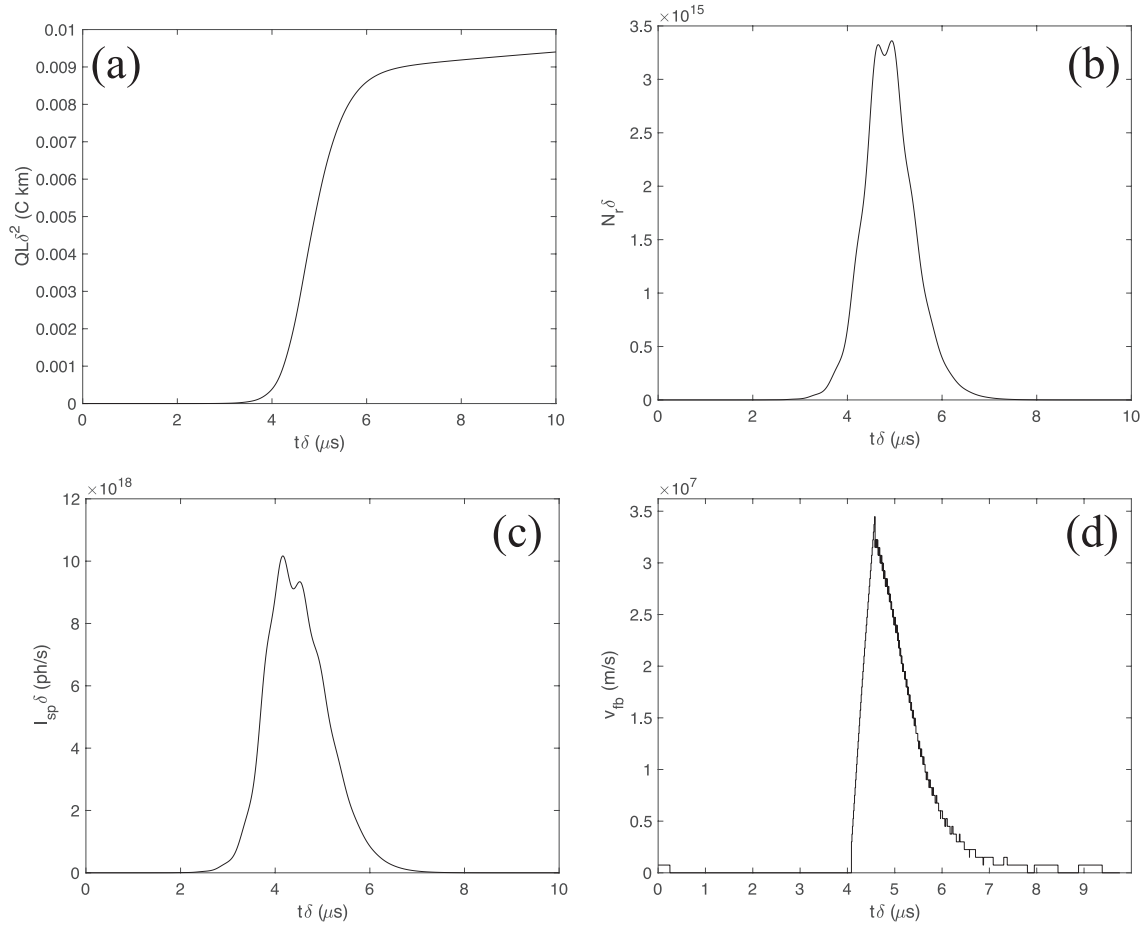

Figure 3. (a) The reduced dipole moment $QL\delta^2$; (b) the reduced total number of runaway electrons $N_r\delta$; (c) the reduced emission intensity of the second positive band system of N_2 $I_{sp}\delta$; and (d) the fast breakdown velocity v_{fb}. The quantities are shown as a function of reduced time $t\delta$ for the case of $d\delta = 150$ m, $E_a/\delta = 12.5$ kV/cm at altitude $h = 11$ km, and the assuming continuous ambient source of runaway electrons S_0.

et al. (2023). The case of $d\delta = 150$ m and $E_a/\delta = 12.5$ kV cm^{-1} at altitude $h = 11$ km is chosen to illustrate model results in Figures 1–3. The first set of results reported in Figure 1 is presented for a case of a continuous ambient source of runaway electrons. For $h = 11$ km $\delta = 0.275$ and for this case $E_a = 3.438$ kV cm^{-1} and $\rho_s^+ = \varepsilon_0 E_a = 3.042 \times 10^{-6}$ C m^{-2}, where ε_0 is permittivity of free space. The charge over $d \times d$ transverse area is $Q = d^2\rho_s^+ = 0.9051$ C ($Q\delta = 0.2489$ C). The relativistic feedback discharge generates plasma space charge densities of positive and negative polarity schematically depicted in Figure 1a as ρ_p^+ and ρ_p^-, respectively. The distribution of these charges is dictated by the discharge dynamics, but they always sum to exact zero as no charge is allowed to leave the domain. The overall dynamics of the discharge is to produce screening of the applied electric field E_a, as illustrated in Figure 1b. In practical calculations, the negative charge supplied by electrons and negative ions accumulates in the form of surface charge density at $z = 0$. The process is analogical to that observed in dielectric barrier discharges (Boeuf, 2003). Toward the end of the simulation, the net positive and negative charges have magnitude $Q\delta = 0.2478$ C ($Q = 0.9011$ C) at $t\delta = 10$ μs that is close to the source value mentioned above (i.e., $Q\delta = 0.2489$ C), but not exactly equal to that value since at $t\delta = 10$ μs system is not fully relaxed yet. The runaway electrons contribute to the negative surface charge. In air, the stopping distance of runaway electrons is $l_e\delta \leq 10$ m (Figure 2c in Pasko, Celestin, et al., 2023). This is much shorter than the considered domain $d\delta = 150$ m, and the present modeling approximates the corresponding charge by the surface charge density at $z = 0$ as explained above.

The principal time scales of the considered feedback discharge can be understood by considering time required for runaway electrons to cover the gap distance $d\delta/c$, where c is the speed of light in free space. At altitudes $h = 0$ km,

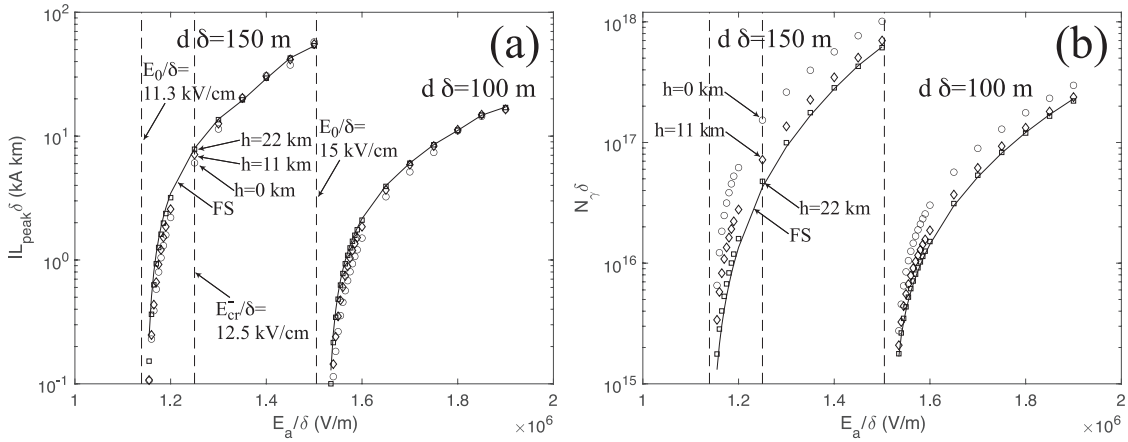

Figure 4. (a) The reduced peak current moment $IL_{peak}\delta$. (b) The reduced total number of emitted gamma ray photons $N_\gamma\delta$. The quantities are shown for reduced gap sizes $d\delta = 100$ and 150 m as a function of reduced applied electric field E_a/δ and for three altitudes $h = 0$ km (circles), 11 km (diamonds), and 22 km (squares). The vertical dashed lines show corresponding relativistic feedback threshold values E_0/δ for the chosen gap size values, and the reference value $E_{cr}^{-}/\delta = 12.5$ kV cm^{-1}. The solid lines show full similarity (FS) solutions obtained assuming $\nu_{a3} = 0$ (see text).

$h = 11$ km, and $h = 22$ km, the reduced gap size $d\delta = 150$ m corresponds to $d = 150$ m, $d = 545$ m, and $d = 3$ km, and d/c values of 0.5, 1.82, and 10 μs, respectively. The results shown in Figures 1 and 2 indicate that the principal relaxation phase of the field and duration of gamma ray pulses and currents the system generates is on the order of $2/\delta$ μs or two round trips over the domain $d\delta$ with speed of light. We note that the present modeling does not account for finite time required for X-ray feedback photons to propagate toward the seeding region (i.e., this propagation is assumed to be instantaneous, see Appendix A). The pulses are expected to be longer due to the additional time on the order of d/c required for the photon transport. This does not affect any principal conclusions of this work. The relaxation of the electric field is illustrated in Figure 1b. We note that for $d\delta = 150$ m domain, the applied field $E_a/\delta = 12.5$ kV/cm in this model example exceeds the feedback threshold field $E_0/\delta = 11.3$ kV/cm by 10.6%. The positive charge density during the relaxation has a distributed form shown in Figure 1c. In Figure 1d, the growth of runaway electrons is saturated when their density reaches maximum value $n_r/\delta^2 \simeq 7.45 \times 10^9$ m^{-3}. The time growth of n_r proceeds in a form of sequential passages of runaway avalanches through the entire domain seeded by the photoelectric feedback photons. During the last cycle with duration $d\delta/c$, when space charge effects become important, the electric field relaxes (see $t\delta = 6$ and 7 μs in Figure 1b) and the system decays as it is no longer able to satisfy the feedback conditions for the growth (see drop in n_r for $t\delta = 6$ and 7 μs in Figure 1d). At this stage, the plasma conductivity σ is mostly defined by the low-energy electron population with density n_e, which is determined by balance of the production rate due to runaway electrons and their loss in two- and three-body attachment collisions $n_r\nu_r^* = (\nu_{a2} + \nu_{a3})n_e$ (see Appendix A). Having equalized d/c to the dielectric relaxation time scale, ε_0/σ leads for the case shown in Figure 1d to $n_{rmax} = \varepsilon_0(\nu_{a2} + \nu_{a3})c/(dq_e\mu_e\nu_r^*) = 7.35 \times 10^9$ m^{-3} in good agreement with modeling. Similar formulas for n_{rmax} have been previously given in Dwyer (2007) and Gourbin and Celestin (2024a). The numerical value is consistent with results obtained in a recent relativistic electromagnetic particle in cell hybrid Monte Carlo simulations (Gourbin & Celestin, 2024b). The current distribution shown in Figure 1e occupies approximately a third of the gap d and represents a compact radiation source for observational distances of tens of kilometers away. Without loss of generality, the spatial distribution of related current moment can be approximated by either a constant or a half sinusoid with zero values at the current extremities (Pervez et al., 2024a). Figure 1f demonstrates very fast dynamics of electrons due to their production and attachment losses. The positive and negative ions dominate the conductivity at $t\delta = 6$ and 7 μs, respectively. These remnant conductivity perturbations due to ions $\sigma_i/\delta \sim 2 \times 10^{-6}$ S/m, corresponding to the dielectric relaxation times $\tau_\sigma\delta = \varepsilon_0/\sigma_i \sim 4.6$ μs, may facilitate seeding of space leaders and lightning initiation. The applied field $E_a/\delta = 12.5$ kV/cm is sufficient for propagation of both positive and negative streamers (see discussion in Pasko, Celestin, et al., 2023) and abundance of electrons present for ~1 μs/δ at initial stage of this discharge will seed development of streamers that require only ~10 ns/δ for their initiation (Liu & Pasko, 2004). As part of model calculations, we also traced the time-dependent position corresponding to $\max(n_eE)$ where the maximum of streamer-generated VHF emissions are expected to occur. Due to the

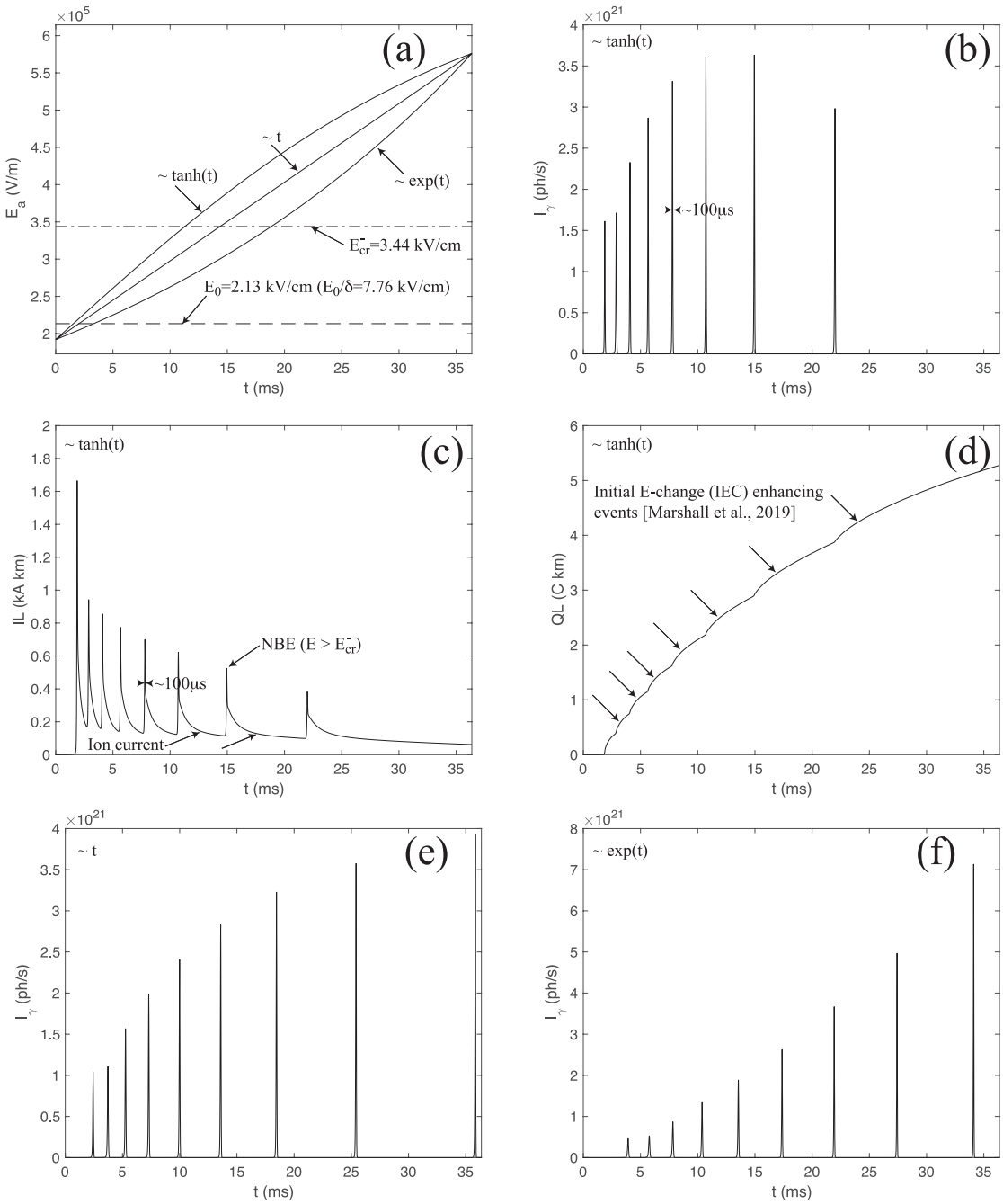

Figure 5. (a) Three different model time dependencies for the applied field E_a (the time and the field are shown in nonreduced form) for the case of $d\delta = 300$ m at altitude $h = 11$ km, and assuming a continuous ambient source of runaway electrons S_0. (b) The emission intensity of gamma rays I_γ. (c) The nonreduced current moment IL. (d) The nonreduced dipole moment QL. In panels (b)–(d), the quantities are shown as functions of nonreduced time t and for slowly increasing E_a/δ from $0.9E_0$ at $t\delta = 0$ to $2.7E_0$ at $t\delta = 10$ ms using hyperbolic tangent function illustrated in panel (a). The horizontal dashed line in panel (a) shows the relativistic feedback threshold value E_0 (for the $d\delta = 300$ m gap), and the horizontal dash-dot line shows value of E_{cr}^-; both are for the $h = 11$ km altitude. Panels (e) and (f) illustrate gamma ray photon intensities in a format similar to that of panel (b) but for linear and exponential time dependencies of E_a, respectively, illustrated in panel (a).

predominance of electrons in conductivity during this fast stage, this position directly corresponds to progression of the peak of the current seen in Figure 1e. During the interval between $t = 5/\delta$ μs and $6/\delta$ μs, the current peak covers distance approximately $15/\delta$ m corresponding to average velocity that can be estimated as 1.5×10^7 m/s. We refer to this velocity as fast breakdown velocity v_{fb} (Rison et al., 2016). For results shown in Figure 1, the peak

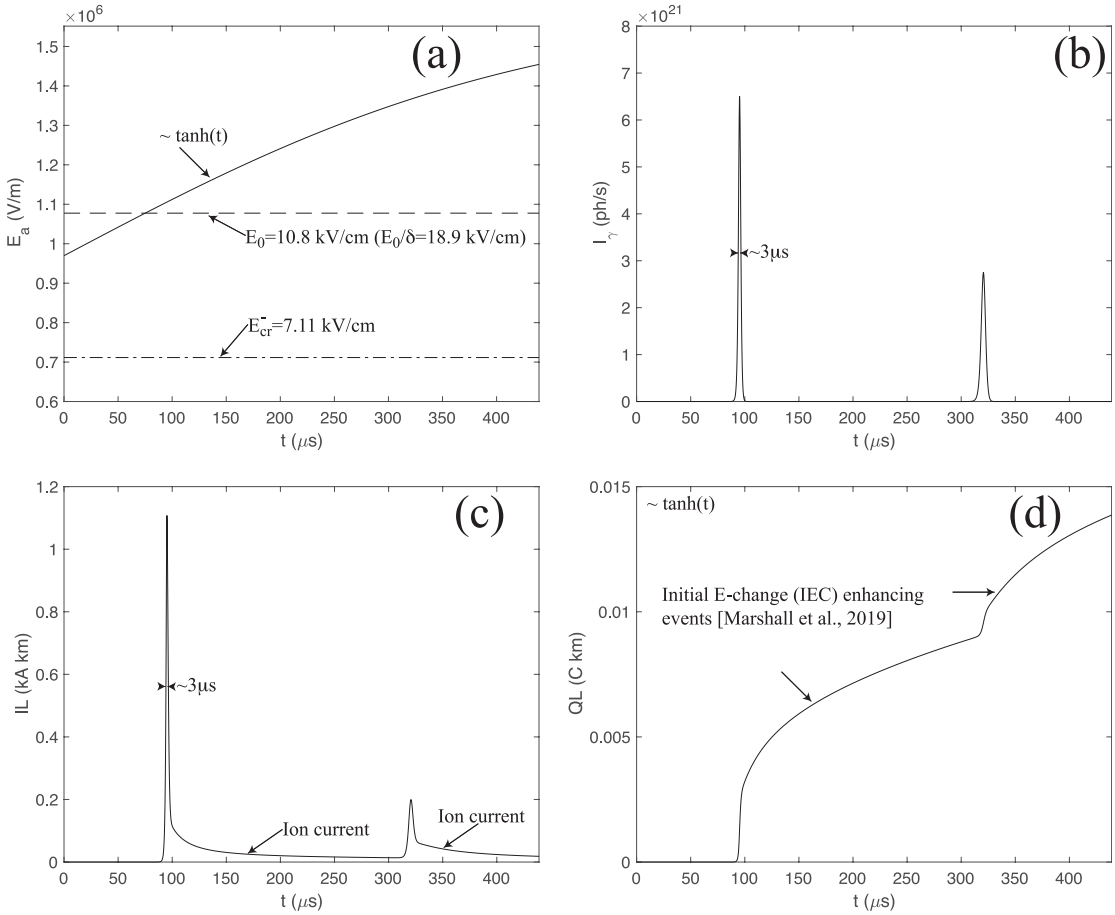

Figure 6. (a) The model time dependence for the applied field E_a (the time and field are shown in nonreduced form) for the case of $d\delta = 75$ m at altitude $h = 5$ km and assuming the continuous ambient source of runaway electrons S_0. (b) The emission intensity of gamma rays I_γ. (c) The nonreduced current moment IL. (d) The nonreduced dipole moment QL. In panels (b)–(d) the quantities are shown as functions of nonreduced time t and for slowly increasing E_a/δ from $0.9E_0$ at $t\delta = 0$ to $1.8E_0$ at $t\delta = 250$ μs using hyperbolic tangent function illustrated in panel (a). The horizontal dashed line in panel (a) shows the relativistic feedback threshold value E_0 (for the $d\delta = 75$ m gap), and the horizontal dash-dot line shows value of E_{cr}^-, both for the $h = 5$ km altitude.

value of v_{fb} is 3.45×10^7 m/s in good agreement with observations (Pu & Cummer, 2024; Rison et al., 2016; Tilles et al., 2019, 2020). The full waveform of $v_{fb}(t)$ is included as Figure 3d.

Figures 2a and 2b illustrate time dynamics of current moments and gamma ray photon fluxes that have the same time scales as discussed above (approximately two round trips with speed of light). The results are illustrated for the cases of one seed runaway electron and the continuous ambient source of runaway electrons. As expected on physical grounds, the initiation of a system with a continuous source S_0 produces a smoother waveform than an initiation with a 1 per m^3 seed placed at $z = d$ (see discussion in Appendix A). The sharp pulsations with rise and fall times on the order of $0.1/\delta$ μs (HF band frequencies 10δ MHz) correspond to the final two to three e-folding lengths l_r/δ of individual runaway electron avalanches when they start making measurable contribution to the current. These pulsations are an intrinsic property of these discharges. For the simulation results shown in Figure 2a, the current is mostly carried by low-energy electrons with runaway electrons contributing ~3% of the total current. It is remarkable that careful inspection of smooth current moment $IL\delta$ waveform obtained even with continuous source S_0 in Figure 2a indicates that these pulsations are also present in this case. Panels (c) and (d) in Figure 2 provide time derivative of these waveforms, which is directly proportional to the radiation field components, to illustrate the presence of these pulsations. This provides explanation for the fine pulsations routinely seen in IBP/NBE/EIP waveforms reviewed in the introduction section (Belz et al., 2020; Chen et al., 2024; Karunarathne et al., 2021; Liu et al., 2022; Marshall et al., 2013; Nag & Rakov, 2010; Pu et al., 2019; Rison et al., 2016; Stolzenburg et al., 2013, 2016). We emphasize that these short pulsations effectively modulate (or are

embedded in) each short waveform, with these waveforms forming various longer time sequences. These can appear as a growing sequence of initial breakdown pulses (IBPs) leading eventually to lightning initiation (e.g., Liu et al., 2022), or a weaker pulse sequence following a stronger NBE-like pulse (e.g., Chen et al., 2024). Chen et al. (2024) refer to modulating/embedded pulsations as ringing, and to the sequence of weaker pulses following their NBE events as secondary pulses. The occurrence of both of these dynamics (i.e., growing and decaying) is of special interest as, in accordance with analysis we present in Section 4.3, these represent a sensitive indicator of the rate of growth of thundercloud electrification.

The pulsations observed in the photoelectric feedback discharges in Figure 2 have direct physical analogy with pulsations in positive corona discharges that proceed on nanosecond time scales at ground pressure (Jansky et al., 2025). In both cases, a discreteness of the initiating electron avalanche (either conventional or relativistic) provides maximum deposition of seed electrons in the source region (either due to the photoionization or due to the photoelectric effect, respectively) at the time when the avalanche reaches the stage of maximum growth. The discreteness of this process in time leads to repetition and amplification of these seed-to-full-avalanche cycles observed as characteristic pulsations embedded in reported waveforms. Understanding of these fine pulsations represents one of the important contributions of this work. In real geophysical situation, the seeding of these pulsations is expected to have a random component due to random appearance of cosmic ray secondaries. We quantitatively demonstrate these pulsations in our work by using two limiting cases: homogeneous seeding of runaway electrons and a single runaway electron seed. The reported mechanism is not sensitive to the initial density of high-energy seed electrons; however, we emphasize that the proposed process would not initiate any discharge in the absence of these seed electrons. The proposed mechanism is therefore broadly consistent with recent findings of lightning initiation events, including fast positive breakdown followed by the fast negative breakdown (discussed in more detail in Section 4.4 below), as being preconditioned by cosmic-ray shower events (Shao et al., 2025). The discussed fine pulsations represent growth of individual relativistic runaway electron avalanches that map to time-dependent currents and radiated waveforms. The short time scales we report $0.1/\delta$ μs are clearly different from those produced by the large-scale (domain size ~5 km) relativistic feedback discharges studied in association with propagating lightning leaders (Dwyer, 2012; Liu & Dwyer, 2013) and in association with thundercloud electrification (Dwyer, 2025).

We note that the system produces longer pulses for lower applied electric fields. However, the relativistic feedback produced pulses that cannot be shorter than the scales discussed above. Thus, when measurable, the time scale of these pulsations can be used to infer the multiplicative spatial scale of the avalanching runaway electrons l_r/δ and applied electric field E_a/δ. The peak current moment in Figure 2a for the continuous source is $IL_{peak}\delta = 7.1$ kA km, and the total number of emitted gamma ray photons corresponding to I_γ in Figure 2b is $N_\gamma\delta = 7.18 \times 10^{16}$. The peak number of produced runaway electrons is $N_{rpeak}\delta = 3.36 \times 10^{15}$, and related time dynamics is illustrated in Figure 3b.

For the model case illustrated in Figure 1, a discharge process would need to generate a dipole moment $Qd = 0.4937$ C km with direction opposite to that generating the applied field to fully compensate the applied electric field. From the simulation results shown in Figure 3a, the dipole moment generated by the discharge at the end of simulation is $QL\delta^2 = 0.0094$ C km and $QL = 0.1243$ C km. This dipole moment is of the same order of magnitude as generated by strong NBEs (Rison et al., 2016) and also by initial electric field changes (IECs) reported in Chapman et al. (2017) and Marshall et al. (2014, 2019). The effective dipole length produced by the discharge is $L = QL/Q = 138$ m, where $Q = 0.9011$ C as was already mentioned at the beginning of the results section. This L is only a fraction of the total gap $d = 545.45$ m in this model case.

The total number of photons corresponding to the second positive band system of N_2 for the continuous model case shown in Figures 1, 2a, and 2b is $N_{sp}\ \delta^2 = 4.39 \times 10^{12}$. The related waveform $I_{sp}(t)$ is included in Figure 3c. The $N_{sp}\ \delta^2 = 4.39 \times 10^{12}$ value when compared to $N_\gamma\delta = 7.18 \times 10^{16}$ would not produce a detectable signal for a 1 cm^2 area photodiode photometer used by the FORTE satellite (Kirkland et al., 2001). We note that the FORTE passband 400–1,100 nm had a 40% reduced sensitivity at 400 nm (Kirkland et al., 2001), but would still allow unbiased detection of bands of this band system extending up to 450 nm if this band system were strong enough for detection. The same conclusion can be made for the first negative band system of N_2^+, whose strong (0,1) 427.8 nm band falls in the same interval, as these emissions do not exceed the strongest (0,0) 337.1 nm band of the second positive band system (Liu & Pasko, 2004; Xu et al., 2015). We reiterate again the point made above that

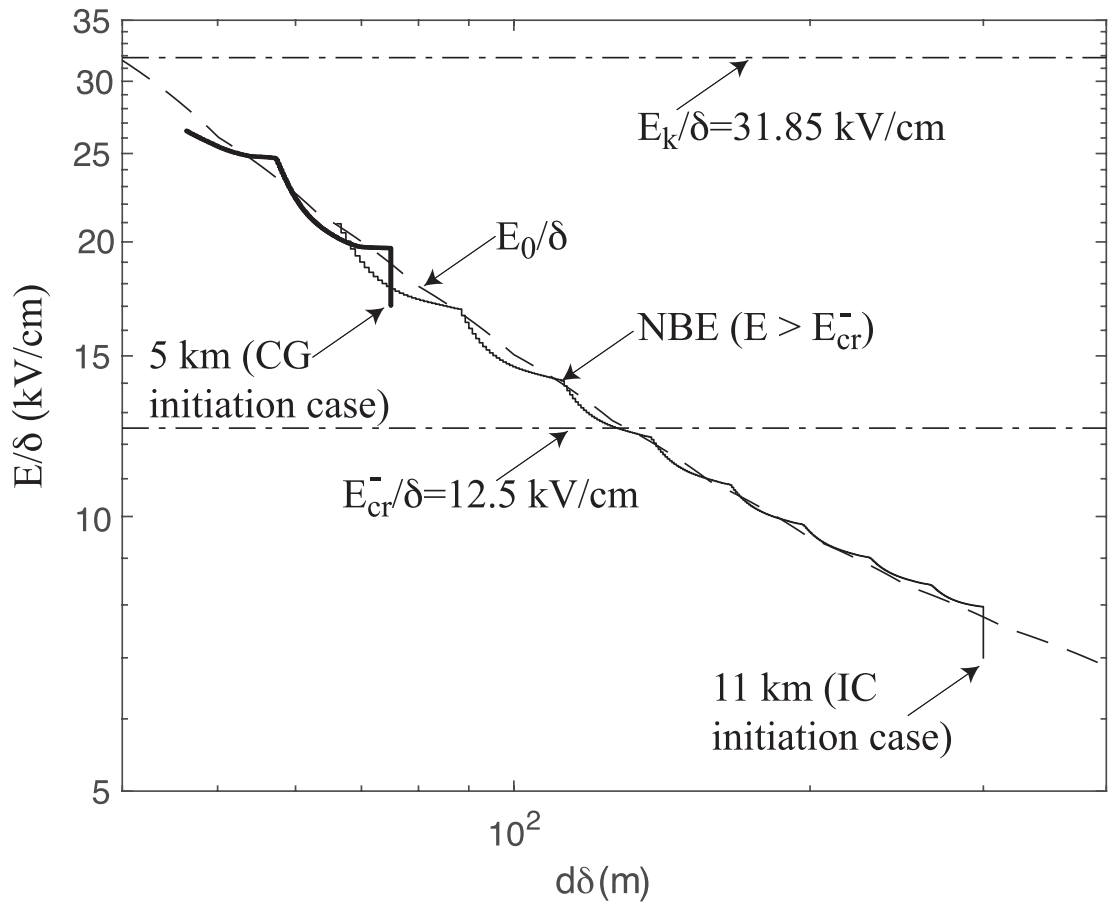

Figure 7. Thin and thick solid lines depict evolution of applied electric field E_a/δ as a function of effective gap size $d_{eff}\delta$ (see text) for the hyperbolic time variation cases shown in Figures 5 and 6, respectively. The dashed line shows relativistic feedback threshold field E_0/δ as a function of reduced gap size $d\delta$ in a format similar to that of Figure 3 in Pasko, Celestin, et al. (2023) and Figure A1a of the present work. The horizontal dot dashed lines show the conventional breakdown threshold E_k/δ and the minimum negative streamer propagation E_{cr}^-/δ fields.

similarly to FORTE, the passband 400–900 nm in Kieu et al. (2024) would not allow the detection of a (0,0) 337.1-nm s positive band of molecular nitrogen N_2. However, it would allow detection of a strong (0,1) 427.8 nm band of the first negative band system of N_2^+. The 427.8 nm emission has not been detected in Kieu et al. (2024). Our results therefore support ideas that the relativistic discharges by themselves are dark (often referred to as dark lightning in previous publications (Alnussirat et al., 2023; Dwyer et al., 2013)). In the present work, we discuss the conditions when relativistic feedback discharges proceed with and without intense streamer activity. The streamers similarly to relativistic feedback discharges are nonthermal discharges. At near-ground air pressures, streamers have a peculiar feature of producing very bright and primarily blue molecular emissions (the second positive band system of molecular nitrogen N_2 and the first negative band system of N_2^+) from the localized regions in their heads. These are still not as bright as atomic emissions produced from channels of thermalized leaders and return strokes. Therefore, following discussion in Rison et al. (2016), we speculate that the VHF producing streamers existing in the same physical space as relativistic feedback discharges appear to be optically dim when explored with instruments having 400–1,100 nm passbands (Jacobson et al., 2013; Kirkland et al., 2001) designed primarily for detection of bright 777.4 nm atomic oxygen emissions from hot thermalized channels of lightning leaders and return strokes. We emphasize that there is now an abundant evidence that NBE discharges are associated with clearly detectable blue emissions observed by blue-sensitive orbiting photometers and imagers (Chou et al., 2018; Li et al., 2023; Liu et al., 2018).

Figures 4a and 4b document the peak values of the current moment $IL_{peak}\delta$ and the total number of emitted gamma ray photons $N_\gamma\delta$ for two gap dimensions $d\delta$ = 100 and 150 m as a function of applied electric field E_a/δ and at three representative altitudes h = 0, 11, and 22 km. We note that $N_\gamma \sim 3 \times 10^{16}$ is a good reference value for

detected TGF events that corresponds to 1 photon per cm^2 at nominal 500-km satellite distance (Carlson et al., 2010). The values shown in Figure 4b are consistent with and exceed this threshold. Typical values of $IL_{peak}\delta$ obtained at closer distances from the sources range from 1 to 10 kA km (Karunarathne et al., 2019; Rison et al., 2016; Tilles et al., 2019). Given the noise levels seen in these data and lightning events (Lyu et al., 2019; Rison et al., 2016), the signals as low as 0.01–0.1 kA km should be detectable. However, the detectability is expected to degrade with increased distance. An interesting result that can be seen from Figures 4a and 4b is that the current moments, that are at the detectability threshold (i.e., 0.1 kA km), still produce TGFs with abundant numbers of photons $\left(N_\gamma\delta \simeq 10^{15}\right)$, that should be easily observable at a close range. Such weak TGFs have been observed at a close range from a high-altitude aircraft (Bjorge-Engeland et al., 2024) and from the ground (Abbasi et al., 2018, 2024; Belz et al., 2020). We note that some of these events occur at later stages of lightning discharge (but before the return stroke) (e.g., Abbasi et al., 2018), and may relate to leader stepping processes.

The reported features in Figures 1–3 are consistent with observations of narrow bipolar events (NBEs) with ~10 μs durations (Nag & Rakov, 2010; Nag et al., 2010; Rison et al., 2016). In Figure 4, we explicitly show by a vertical dashed line the threshold field for streamer growth E_{cr}^{-}/δ. It is clear from this figure that very weak and very strong photoelectric feedback discharges can be produced with and without VHF producing streamers, depending on whether the applied field appears above or below the E_{cr}^{-}/δ threshold. We suggest that very weak discharges with and without VHF pulses (many would remain undetectable due to their weakness) can be produced, and those that were detected were recorded at very close range as in Chapman et al. (2017) and Marshall et al. (2014, 2019). As noted above, these discharges definitely scale with altitude. They last longer in time and are associated with higher dipole moment changes at higher altitudes (Belz et al., 2020). It is generally understood that the electric field needed to initiate lightning scales proportionally to air density and is reduced with increase of altitude (Marshall et al., 1995). The gas discharges proceed faster at lower altitudes due to increase in (proportional to the air density) frequencies of two body collisions involving electrons. These involve both production (i.e., ionization) and loss (i.e., attachment). It is reasonable to hypothesize that electric field fluctuations proceed on a variety of time scales at all altitudes, and only fast electric field enhancements can overcome fast electron losses at high air pressures at lower altitude in comparison with higher altitudes in the Earth's atmosphere. These field enhancements are not likely to last a long time and therefore are difficult to observe locally. The highest inferred fields do not exceed $\sim E_k/3$ (Stolzenburg et al., 2007, and references therein), where E_k is the conventional breakdown threshold field defined by the equality of ionization and attachment frequencies of electrons in air. In the present work, we adopt $E_k/\delta = 31.85$ kV/cm (Jansky et al., 2025). It is possible that lower air pressure is responsible for making some of the events longer at higher altitudes. In some published data sets, the longer duration ~50 μs EIPs (Tilles et al., 2020) clearly appear at higher altitudes than lightning initiating NBEs, and therefore, air pressure could be at least partially responsible for their longer duration. Additional factors are likely related to the upward progression (on km scales) of the stepping negative leaders (Heumesser et al., 2021; Kohn et al., 2020; Lu et al., 2010) leading to significant increase of their potentials and lengths of their streamer zones and providing robust conditions for feedback discharges (Pasko, Celestin, et al., 2023). In the abovementioned contexts, the analysis of similarity scaling of photoelectric feedback discharges with atmospheric air density (altitude) is of special interest and is discussed in the next subsection.

4.2. Similarity Scaling of Photoelectric Feedback Discharges as a Function of Air Density

The similarity laws are useful for understanding how different parameters of the discharge change with ambient gas density. In this paper, the ambient air density variations are described using parameter δ introduced at the beginning of the Model Formulation section. The applied electric field scaling E_a proportionally to δ, mentioned above, is one of the many similarity relations. It is inferred that the ratio E_a/δ remains constant in similar discharges and the field in this form is referred to as reduced field. All physical quantities presented in Figures 1–4 and related discussion in previous sections of this paper are expressed in their reduced form. A review of similarity relationships and physical grounds for these relationships can be found in Pasko (2006, and references therein). The scaling of parameters discussed in this work (see full summary in Appendix A) with reduced air density parameter δ can be summarized as follows: time $t \propto 1/\delta$, length $d \propto 1/\delta$, electric field $E \propto \delta$, mobilities of electrons and ions $\propto 1/\delta$, all frequencies (except three-body attachment) $\propto\delta$, charge density ρ and densities of electrons (including runaway electrons) and ions $\propto\delta^2$, current density $J \propto \delta^2$, conductivity $\sigma \propto \delta$, current moment $IL \propto 1/\delta$, charge $Q \propto 1/\delta$, dipole moment $QL \propto 1/\delta^2$, total number of runaway electrons $N_r \propto 1/\delta$, total number of gamma ray photons $N_\gamma \propto 1/\delta$, second positive band system of N_2 emission intensity $I_{sp} \propto 1/\delta$, and the total number

of related photons $N_{sp} \propto 1/\delta^2$. The gamma ray emission intensity I_γ, the current I, the velocities of electrons and ions (including runaway electrons), the derivative $\frac{d}{dt}(IL)$, and the fast breakdown velocity v_{fb} do not scale. Since velocity is scale-invariant, the density is proportional to current divided by area (area scales as $\propto 1/\delta^2$), and therefore density scales as $\propto \delta^2$, as already noted above. The δ parameter reduces by a factor of 3 between 6 and 14.2 km, and by a factor of 20 between ground and 22 km altitude. This gives significant increase with altitude to some observables, such as the total number of emitted gamma ray photons N_γ. Of special interest is the scaling of dipole moment $QL \propto 1/\delta^2$ that should result in a significant increase in the quasi-static component of the electric field from these discharges when measured at a close range. The total number of photons N_{sp} of the second positive band system also gets a significant $1/\delta^2$ boost with increase in altitude. However, given quantitative results reported below, this generally does not provide a sufficient increase to make it comparable to N_γ at thundercloud altitudes. The full similarity (FS) of reported results (i.e., numerically identical results when expressed in the above listed scaled form) is achieved when the ambient source of runaway electrons S_0 is scaled as $\propto \delta^3$ and at altitudes where the three-body attachment of electrons becomes insignificant in comparison with the two-body attachment. Since specific values of S_0 do not affect any principal results of this work (beyond introducing simple time shifts in model pulse onset times, see additional discussion in Appendix A), in all reported calculations, we assumed the $\propto \delta^3$ scaling. The three-body attachment introduces measurable deviations from the full similarity solutions as illustrated by results in Figures 4a and 4b. The $N_\gamma \delta$ values are increased at lower altitudes due to increase in n_{rmax} that is proportional to ν_{a3} as explained above (Figure 4b), and the peak current moment $IL_{peak}\delta$ is diminished due to additional electron losses at low altitudes (Figure 4a, open circles corresponding to $h = 0$ km appear below diamonds ($h = 11$ km), and diamonds appear below squares ($h = 22$ km)). Figure A1b provides distribution of the reduced electric field E/δ as a function of altitude corresponding to the condition $\nu_{a3} = \nu_{a2}$. For a representative value of $E_a/\delta = 12.5$ kV cm^{-1} chosen for model analysis in this work two-body attachment frequency exceeds three-body attachment frequency ($\nu_{a2} > \nu_{a3}$) above altitude $h \simeq 9$ km.

4.3. FGFs and Initial Electric Field Change (IEC) Enhancing Events

In this section, we demonstrate that sequence of flickering gamma ray flashes (FGFs) reported in Fishman et al. (1994) and Ostgaard et al. (2024) and weak electric field changes (Chapman et al., 2017; Marshall et al., 2014, 2019) can be quantitatively explained using the same photoelectric feedback principles that we formulate in this work. The effects are demonstrated by increasing E_a as a function of time with different rates and different model-defined functional dependencies on time, and physical quantities are shown in nonreduced form to facilitate comparison with observations.

Figure 5a provides three model examples for a gradual hyperbolic tangent, linear and exponential field growth cases assuming $d\delta = 300$ m at altitude $h = 11$ km, and continuous ambient source of runaway electrons S_0. The starting applied electric field in this model case is $0.9E_0 \simeq 2 \times 10^5$ V/m as can be seen in Figure 5a. The estimated source charges of positive and negative polarity creating an applied field in this case have magnitude $Q = 2.1$ C. We emphasize that it does not matter how fast this charge is generated and what is preceding time history of this charge buildup (it may take hundreds of ms or tens of seconds to accumulate this charge). The triggering of photoelectric feedback discharges occurs with a very small increment of the electric field above the E_0 threshold as results in Figure 4 demonstrated. For example, a 1% increase in this source charge over 20 ms interval would be sufficient. This would correspond to a ~1 A charging current fluctuation applied over 20 ms. The example in Figure 5a corresponds to approximately 100 A charging current as it doubles the field 2×10^5 V/m in about 20 ms. This leads to the intense sequence of gamma ray pulses with duration of approximately 100 μs each (measured at half magnitude level) as shown in Figure 5b. Each pulse in this model case corresponds to approximately 2×10^{17} gamma ray photons as can be directly estimated from Figure 5b. The readers can scale the results shown in Figure 5 to any other altitude of interest using similarity relationships reviewed in the previous section. For example, at 22 km altitude, the air density is factor 5.5 lower than at 11 km, and the pulse duration will be approximately 0.55 ms; duration of this entire pulse sequence will be 0.2 s, and the total number of emitted gamma ray photons in each pulse is $\sim 10^{18}$. Panel (c) in Figure 5 illustrates time dynamics of current moment IL. Each gamma ray pulse corresponds to relatively strong peak current moment on the order of ~1 kA km. It is interesting to note that there is a continuous nonzero current flow between gamma ray pulses that is facilitated entirely by positive and negative ions (negative ions are formed by quick attachment losses of electrons as was illustrated in Figure 1f). This directly

translates to periods of continuous growth of the dipole moment QL between fast changes corresponding to gamma ray pulses as can be seen in Figure 5d. These dynamics of QL would translate to changes of quasi-static electric fields, if observed at a close range. We suggest that this provides a straightforward explanation of initial E-change (IEC) enhancing events observed in Chapman et al. (2017) and Marshall et al. (2014, 2019). The model case in Figure 5 resembles multiple TGF pulses (referred to as FGFs) observed with separations of several milliseconds reported in Fishman et al. (1994) and Ostgaard et al. (2024). As we further discuss below, the observed pulsations are produced as the increasing field progressively satisfies the relativistic feedback threshold for shorter and shorter gaps (where with each pulsation, an additional part of the gap is occupied by a conducting region containing positive and negative ions). The periodicity of pulsations is a sensitive function of the slope of the increasing electric field. Panels (e) and (f) of Figure 5 give additional examples for linear and exponential field growth cases, respectively, with driving field waveforms shown in Figure 5a. We note a factor of two increase in photon intensity scale in exponential case (panel (f)). For a more gradual increase of the field in time, the magnitude of pulsations is reduced (both IL_{peak} and N_γ) and the duration of each pulse and the separation between pulses become longer. Long duration ∼1–10 sec X-ray pulses in and above thunderclouds were reported in Eack and Beasley (2015) and Eack et al. (1996), and we suggest that this progression naturally evolves into a gamma ray glow regime (e.g., Parks et al., 1981; Tsuchiya et al., 2013; Wada et al., 2021; Marisaldi et al., 2024, and references therein). As we already noted above and discussed in Pasko, Celestin, et al. (2023), it is likely that the strongest TGFs are produced by stepping of negative lightning leaders that would provide fast increase of the field above the relativistic feedback threshold in their negative streamer zones and not during gradual growth of the field.

The results shown in Figure 5 for 11 km altitude can be linked to initiation of IC discharges. We now illustrate a discharge developing at lower altitude of 5 km and on shorter time scale of approximately 400 μs that could be linked to initiation of CG discharges. This model case uses hyperbolic tangent field growth waveform shown in Figure 6a, assumes a gap size $d\delta = 75$ m, and uses a continuous ambient source of runaway electrons S_0. The starting applied electric field in this model case is $0.9E_0 \simeq 10^6$ V/m as can be seen in Figure 6a. The estimated source charges of positive and negative polarities creating applied field in this case have magnitude $Q = 0.154$ C. As can be directly seen from the figure in this model case, ∼10% of this charge increase (i.e., ∼0.0154) occurs on time scale of approximately 100 μs, and similarly to case shown in Figure 5, the source current fluctuation required in this scenario is ∼150 A. This model scenario produces two TGF pulses with duration of approximately 3 μs as shown in Figure 6b. Each pulse emits approximately 10^{16} photons that is close but below the nominal 3×10^{16} discussed above required for orbital detection, but an order of magnitude above the highest reported value in ground observations 8×10^{14} (Abbasi et al., 2024) and therefore would be observable from the ground. Cases in Figures 5 and 6 lead to strong TGF emissions, and we emphasize again that there is a very broad parametric space (with orders of magnitude lower source currents) that would lead to weaker 10^{12}–10^{15} total photon TGFs that still would be measurable at a close range (Bjorge-Engeland et al., 2024). Panel (c) in Figure 6 illustrates time dynamics of current moment IL. The first pulse corresponds to a relatively strong peak current moment on the order of ∼1 kA km. There is a continuous nonzero ion current flow between gamma ray pulses as discussed with relation to Figure 6c. The pulse durations and dipole moment QL changes (shown in Figure 6d) in this model case closely resemble ∼0.01 C km IEC-enhancing events for CGs reported in Chapman et al. (2017) and Marshall et al. (2014, 2019).

4.4. Physical Mechanism of NBEs and Fast Negative Breakdown

The model pulsations observed in Figures 5 and 6 are produced as the increasing field E_a/δ progressively exceeds the relativistic feedback threshold field E_0/δ for shorter and shorter gaps, where with each pulsation, an additional part of the gap is occupied by a conducting region containing positive and negative ions. Although this scenario is different from pulsations produced in large-scale discharges (domain size ∼5 km) at lower applied electric fields that are dominated by the positron feedback (Dwyer, 2012, 2025; Liu & Dwyer, 2013), the fundamental physical origin of pulsations in both modeling approaches maybe identical to what we describe in present work, as in all considered scenarios, the system needs continuous growth of the electric field applied to the feedback region for continuation of pulses, and pulsations cease immediately if the growth is terminated. The present work assumes planar geometry of the applied field, and the role of nonplanar geometry on considered feedback processes on different spatial scales requires further investigation. In Figure 7, we explicitly plot the progression of the effective gap dimensions in the course of simulations shown in Figures 5 and 6. The effective gap dimension $d_{eff}\delta$ is traced in time by finding the coordinate where the applied electric field is reduced to the minimum electric field

required for development of relativistic runaway electron avalanche $E_t/\delta = 2.76$ kV/cm (Dwyer et al., 2012, and references therein). Figure 7 shows how both 11 km IC initiation (Figure 5) and 5 km CG initiation (Figure 6) cases closely follow E_0/δ dashed line. The fast positive breakdown solutions driven by the photoelectric feedback that we simulate in this work occur both at applied fields E_a/δ below and above the minimum negative streamer propagation field E_{cr}^-/δ shown by the horizontal dot dashed line in Figure 7. The photoelectric feedback discharges are considered as strong sources of free electrons, and as was already noted above in fields $E_a/\delta > E_{cr}^-/\delta$, streamers develop exponentially and much faster than the photoelectric feedback discharges (Pervez et al., 2024b). Each double-headed streamer injects a dipole moment that is directed opposite to the one creating the applied field, and from this physical perspective, streamers serve exactly the same role in screening the applied electric field as conducting regions created by the photoelectric feedback discharges. In fields $E_a/\delta > E_{cr}^-/\delta$, streamers perform this screening action much faster than photoelectric feedback; however, we suggest that in scenarios of lightning initiation, the photoelectric feedback discharges play a mandatory role in seeding of these streamer discharges. In Figure 5, the streamers are triggered by the seventh pulse as marked in Figure 5c, and we mark this pulse as NBE. For reference, we also included the E_{cr}^-/δ threshold field in Figure 5a and marked the NBE production pulse in Figure 7. In CG case of Figure 6, the streamers are triggered with both the first and the second pulse. In both the IC and the CG scenarios, these pulses are expected to be associated with VHF pulses of the same duration. In present work, we do not model VHF emissions and streamers to leader transition processes. It can be speculated that many of these events do not lead to lightning initiation and occur in isolation. In data sets reported in Ostgaard et al. (2024), the FGF pulses are followed by lightning initiating NBE events, and we suggest that each NBE event still has gamma ray emissions associated with photoelectric feedback discharge that seeded streamers, but the photoelectric feedback discharge has been suppressed due to fast screening of the field by streamers. Streamers by themselves are able to generate runaway electrons and may contribute to seeding of runaway electron avalanches in streamer zones of already developed lightning readers (Celestin & Pasko, 2011; Celestin et al., 2015; Moss et al., 2006). However, in virgin air with no electron seeds, the photoelectric feedback discharges maybe an essential component of the initial breakdown processes leading to lightning initiation. The observed waveforms of emitted sferics, quasi-static fields measured at a close range, photometric and video records, and observations of X-ray emissions reviewed in this paper provide support for this hypothesis.

Our analysis is in agreement with ideas expressed in Huang et al. (2021) indicating that a short and not always easily detectable fast positive breakdown (FPB) event (Rison et al., 2016) with various magnitudes is commonly present as a lightning initiation event. We also support ideas expressed in Liu et al. (2019) noting similarities between sprite halo events and FPB. Liu et al. (2019) indicate that in sprite halo case, the high ambient density of electrons in the lower ionosphere leads to a dynamical response of that system resembling FPB. We suggest that FPB in case of photoelectric feedback discharges produces a lot of seed electrons that can be interpreted as lower ionospheric electrons. In Figure 8, we schematically show this high-conductivity plasmoid region, that occupies only a fraction of the gap d and corresponds to last 2–3 e-foldings of relativistic runaway electron avalanches we discussed with relationship to our results related to Figure 1 above. It is assumed that applied field E_a exceeds the inception of the self-sustained relativistic runaway discharges field E_0 (with variety of magnitudes and time scales as discussed in the model cases discussed above). Figure 8 shows three distinct regimes mentioned already at the end of the Model Formulation section. If $E_0 < E_{cr}^-$, where E_{cr}^- is the minimum negative streamer propagation field, no intense streamer activity can be produced. This regime may or may not involve VHF silent positive streamers and leaders, and covers FGF and gamma ray glow regimes. If $E_0 \sim E_{cr}^-$, VHF noisy negative streamer heads can develop simultaneously with positive streamers following general FPB progression of the photoelectric feedback discharge (also can be referred to as mixed fast breakdown (mixed FB) (Huang et al., 2021)). This regime would normally correspond to a situation in NBEs and to a situation during formation of the negative streamer zone of stepping negative leader (Pasko, Celestin, et al., 2023). If $E_0 > E_{cr}^-$, VHF noisy negative streamer heads can develop simultaneously with positive streamers following general FPB progression of the photoelectric feedback discharge, and VHF noisy negative streamers also can be launched from other remote parts of the gap d not occupied by the original FPB region. Since these other parts of the gap have lower conductivity and electron density, the propagation of negative streamers likely follows development of an extensive network of positive streamers that extends into that region. These positive streamers that accelerate, expand, and branch similarly to what is observed in sprites below the lower ionosphere (Stenbaek-Nielsen et al., 2025), then initiate similarly fast growing, expanding, and branching negative streamers that are observed as spanning significantly larger distances than FPB and are referred to as fast negative breakdown (FNB) (shown in the right part of Figure 8). We

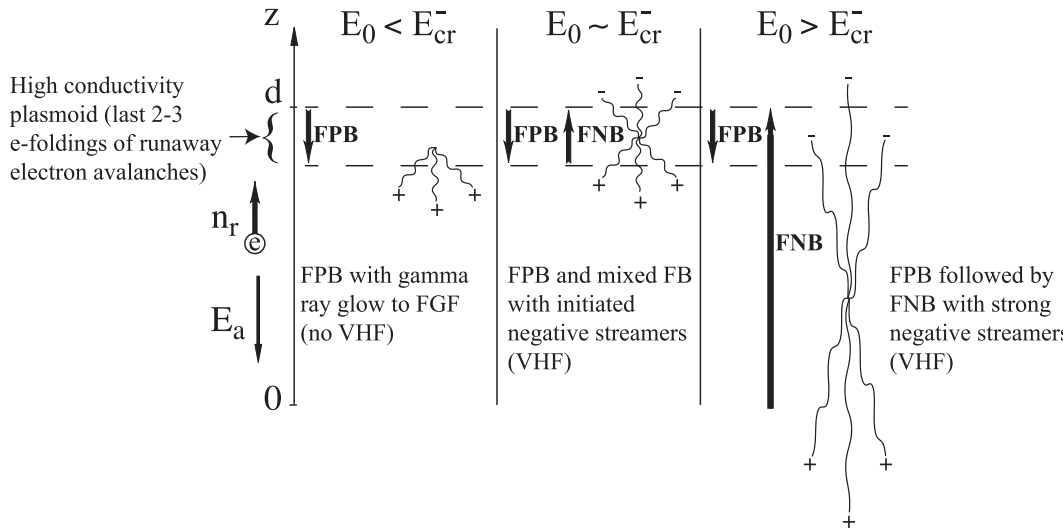

Figure 8. Conceptual representation of conditions required for transition from fast positive breakdown (FPB) to fast negative breakdown (FNB) based on relationship between the relativistic feedback threshold E_0/δ and the minimum negative streamer propagation E_{cr}^-/δ fields.

note that double-headed streamers undoubtedly exist (Liu & Pasko, 2004), but have never been observed in sprites. The reason is that streamers in sprites become visible only after significant exponential growth, and we normally do not see regions of initiation of positive streamers moving downward, and negative streamers appear to be initiating either from already bright positive streamer channels or from not visible regions at lower altitudes. Both types of streamers appear as exponentially growing and eventually branching columns of luminosity, with a typical delay, when negative streamers propagate upward after formation of positive streamers. We suggest that similar dynamics exist in development of FNB. Interested readers can review related video record and imagery in McHarg et al. (2021), Stenbaek-Nielsen et al. (2025), and references cited therein) (https://apod.nasa.gov/apod/ap210104.html).

It is possible to explain various observations of electric and magnetic fields (from quasi-static to approximately VLF-LF) generated by a lightning related phenomena, including short IBP and NBE low frequency waveforms reviewed in the introduction section, by considering the dynamics of currents and charges induced on conducting objects of various conductivities and geometrical configurations subjected to the ambient applied electric field (e.g., Pasko et al., 1998; Pasko, 2014; da Silva & Pasko, 2015; Cummer, 2020; Ueda et al., 2024). It is also possible that VHF noisy streamers, that represent an unquestionable part of experimental data discussed in this paper, are initiated when the ambient electric field fluctuations exceed the conventional breakdown threshold field E_k in small volumes $\sim 10^{-4}$–10^{-3} m^{-3} (Kostinskiy et al., 2020). Having considered the existing knowledge, these streamers should be initiated on very short time scales ~1 μs in 100 × 100 × 100 m^3 volumes (Liu et al., 2022) and given their nominal speeds $\sim 10^6$ m s^{-1}, they do need to be initiated nearly instantaneously in the entirety of the volume (i.e., would not be able to propagate across that volume as it would require time on the order of ~100 m/10^6 m s^{-1} = 100 μs). The streamers are experimentally documented to reach propagation speeds on the order of one tenth of the speed of light ~3 × 10^7 m/s. However, they spend most of their lifetime at much lower velocities, while accelerating to these peak values (e.g., Pervez et al., 2024b; Stenbaek-Nielsen et al., 2025, and references therein). As this work demonstrates, the photoelectric feedback discharges are able to produce strong ionization in the abovementioned volumes and seed streamers on ~1 μs time scales. The existing evidence of hard, multi-MeV, X-ray emissions (Abbasi et al., 2018), with the first-principles experiment-driven modeling values extending to ~60 MeV (Berge & Celestin, 2019), and fine time dynamic details of the fast positive breakdown (Rison et al., 2016), that represents an intrinsic property of the photoelectric feedback discharges as reported in this work above, provide an additional evidence in support of these discharges as a unified physical mechanism of IBPs, NBEs, EIPs, and TGFs.

5. Conclusions

The results presented in this work provide a unified physical mechanism based on photoelectric feedback discharges for IBPs, NBEs, EIPs, and TGFs. There is an experimental evidence of direct time association of TGFs with IBPs (Abbasi et al., 2018; Belz et al., 2020) and with EIPs (Lyu et al., 2016; Neubert et al., 2020; Ostgaard et al., 2021). We explain how VHF and streamer-rich NBEs maybe preconditioned by the optically dark and radio silent photoelectric feedback discharges several milliseconds before occurrence of these events (Ostgaard et al., 2024), and suggest that NBEs should be directly associated in time with low-intensity gamma ray emissions as well. Our results support suggestion of Neubert et al. (2021) that tens of microseconds blue optical pulses observed at 337.1 nm (corresponding to the second positive band system of N_2) are optical fingerprints of NBE sources observed in radio waves. Most recent findings in Liu et al. (2024) lend further support for this hypothesis. We show under which conditions photoelectric feedback discharges, that by themselves are optically dark, may stimulate streamers as existing video imaging of blue jets and pulsating blue jets indicate (Chanrion et al., 2017; Soler et al., 2021).

Appendix A: Numerical Implementation

The runaway electrons with energy ε are characterized by number density n_r and the normalized-to-unity electron energy distribution function $f_e(\varepsilon) = \frac{1}{\mathcal{E}_0} e^{-\frac{\varepsilon}{\mathcal{E}_0}}$ ($\mathcal{E}_0 = 7.3 \times 10^6$ eV) (Dwyer et al., 2012). These electrons avalanche in opposite direction to the applied electric field and their avalanche multiplication is characterized by length $l_r\delta = \frac{1}{E/\delta} \frac{\mathcal{E}_0}{\left(1 - \frac{E_{t_0}}{E/\delta}\right)}$ (Dwyer et al., 2012), where $E_{t_0} = 2.76$ kV cm^{-1}. In present modeling, $l_r\delta$ varies depending on spatial distribution of the electric field $E(z)$. The X-rays are attenuated due to photoelectric absorption, Compton scattering, and pair production. The model approach to the production of secondary relativistic runaway electrons due to photoelectric absorption of X-rays in the volume of air follows the integral formulation described in Pasko, Celestin, et al. (2023), and Pasko, Janalizadeh, and Jansky (2023) and assumes that the distribution of runaway electrons in the discharge volume is mostly controlled by their seeding region at $z = d$ and adopting $S_{pe}(d)$ values for the entire domain, that is, $S_{pe}(z) = S_{pe}(d)$, where S_{pe} is the production rate of runaway electrons in units of m^{-3}s^{-1}. The physical grounds for this approximation are discussed in Pasko, Celestin, et al. (2023, Section 2.1). Figure A1a includes documentation of the related threshold values E_0/δ versus $d\delta$. The deviations from the full solution shown in the same figure do not exceed 2%. The dynamics of relativistic runaway electrons are described by the same continuity equation as shown in Pasko, Celestin, et al. (2023), but with addition of the $\partial n_r/\partial t$ term. The model has provision to initiate the runaway electron population with a seed density of one electron per m^3 placed at $t = 0$ and $z = d$, or continuous ambient source S_0 (m^{-3}s^{-1}) introduced in the entire domain. The rate S_0 can represent seeds generated by radon decay or by the cosmic rays (McCarthy & Parks, 1992; Suszcynsky et al., 1996), or by propagating streamers (Celestin & Pasko, 2011; Moss et al., 2006), depending on the altitude

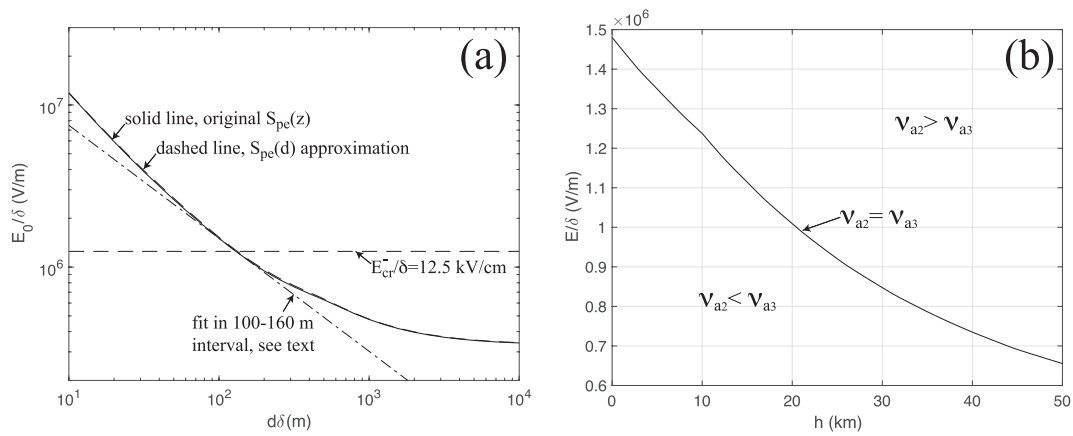

Figure A1. (a) The reduced threshold electric field E_0/δ required for inception of relativistic runaway discharges for different reduced gap sizes $d\delta$ in air (Pasko, Celestin, et al., 2023). (b) The reduced electric field E/δ as a function of altitude h in the Earth's atmosphere corresponding to the equality of two- and three-body attachment frequencies of electrons, that is, $\nu_{a2} = \nu_{a3}$.

and context. The full similarity solutions discussed in the main text correspond to S_0 scaling with atmospheric density as $\propto\delta^3$. In practical calculations including nonzero S_0 values, a value $S_0 = 10\ \mathrm{m^{-3}s^{-1}}$ is assumed at 10 km altitude (McCarthy & Parks, 1992) and scaled $\propto\delta^3$ to other altitudes. The system initiation with a single electron per $\mathrm{m^3}$ leads to more pronounced fluctuations of n_r in time, and variations in magnitude of S_0 lead to shifts in the onset times when space charge effects become important (i.e., the X-ray and current pulses are generated earlier in time if S_0 is increased). This does not affect any conclusions of the present work. The model accurately accounts for all positive and negative charges generated inside of the simulation domain. The sources and multiplication of relativistic runaway electrons add positive ions. A model representation of the friction force acting on relativistic electrons in air against the accelerating force from the externally applied field $F(\varepsilon)$ in eV $\mathrm{m^{-1}}$, shown in Figure 2a in Pasko, Celestin, et al. (2023), can be used to estimate its average over the electron energy distribution $f_e(\varepsilon)$ as $< F > = \int_0^\infty f_e(\varepsilon)F(\varepsilon)d\varepsilon$ (eV $\mathrm{m^{-1}}$). Having assumed the average energy lost per one electron-ion pair production (Dwyer & Babich, 2011) $\varepsilon^* = 34$ eV, leads to $< F >/\varepsilon^* = 7{,}644\ \mathrm{m^{-1}}$ and to effective frequency $\nu_r^* = < F > c/\varepsilon^* = 2.29 \times 10^{12}\ \mathrm{s^{-1}}$, where c is speed of light in free space. Independent calculations of other authors assuming $0.89c$ for average speed of runaway electrons and using $< F >/\varepsilon^* = 8{,}350\ \mathrm{m^{-1}}$ (Babich & Bochkov, 2011; Coleman & Dwyer, 2006; Dwyer & Babich, 2011) leads to similar values $\nu_r^* = 2.23 \times 10^{12}\ \mathrm{s^{-1}}$. For all calculations reported in this work, we adopted $\nu_r^*/\delta = 2.29 \times 10^{12}\ \mathrm{s^{-1}}$. Fully time-dependent versions of continuity equations are used for densities of low-energy electrons n_e, and positive n_p and negative n_n ions (e.g., Liu & Becerra, 2017). The source term $n_r\nu_r^*$ is added to equations for electrons n_e and positive ions n_p. We ignore photoionization effects in air as the related photon absorption scales do not exceed 1 cm at ground pressure (Bourdon et al., 2007; Janalizadeh & Pasko, 2019) and are not important for any physical processes in the 100-m domains considered in this work. Similar to treatments of low-energy electron populations in conventional corona discharges, we ignore electron and ion diffusion, and electron-ion recombination (Liu & Becerra, 2017). Ignoring electron-ion recombination is consistent with analysis in Dwyer (2012). The reduced electron mobility $\mu_e\delta$, the reduced two- and three-body electron attachments ν_{a2}/δ and ν_{a3}/δ^2, the reduced electron impact ionization ν_i/δ, and the reduced electron impact excitation of the molecular nitrogen N_2 $C^3\Pi_u$ state ν_{sp}/δ frequencies are calculated as functions of reduced electric field E/δ using BOLSIG+ software (Hagelaar & Pitchford, 2005; Janalizadeh & Pasko, 2020). The transition rate of the $C^3\Pi_u$ state is assumed to be $A_{sp} = 2 \times 10^7\ \mathrm{s^{-1}}$ (radiative lifetime 0.05 μs), and this state is assumed to be quenched in collisions with molecular oxygen O_2 with quenching rate constant $k_q = 2 \times 10^{-16}\ \mathrm{m^3s^{-1}}$ (da Silva & Pasko, 2013) corresponding to $h_q = 28$ km quenching altitude. The reduced mobilities of both positive and negative ions are assumed to be $\mu_i/\delta = 3\ \mathrm{cm^2V^{-1}s^{-1}}$ (Janalizadeh & Pasko, 2021). The recombination rate constant of negative and positive ions is assumed to be $\beta_i = 2 \times 10^{-13}\ \mathrm{m^3s^{-1}}$ (Kossyi et al., 1992; Liu & Becerra, 2017). The total reduced emission frequency of bremsstrahlung photons per one runaway electron is $\nu_\gamma^t/\delta = 1.67 \times 10^7\ \mathrm{s^{-1}}$, which includes all photons emitted in the energy interval between 1 keV and 100 MeV (Pasko, Celestin, et al., 2023). Most of the conductivity changes and space charge effects normally develop in a region of maximum of n_r that occupies only a fraction of the domain length d. It is assumed that the area d^2 in a plane perpendicular to z represents a reasonable approximation of the discharge transverse extent for which the adopted one-dimensional modeling is valid. In all reported results, it is therefore assumed that effective volume of the discharge is d^3. The reported diagnostics are total number of runaway electrons $N_r(t) = d^2\int_0^d n_r dz$; gamma ray emission intensity $I_\gamma(t) = \nu_\gamma^t N_r(t)$ (photons $\mathrm{s^{-1}}$); total number of emitted gamma ray photons $N_\gamma = \int_0^\infty I_\gamma(t)dt$; charge density $\rho = -q_e n_e - q_e n_r - q_e n_n + q_e n_p$ ($\mathrm{C\ m^{-3}}$), where q_e is absolute value of electron charge; velocities of electrons and ions $v_e = -\mu_e E$, $v_n = -\mu_i E$, $v_p = \mu_i E$ ($\mathrm{m\ s^{-1}}$); current density $J = -q_e n_e v_e + q_e n_r c\ - q_e n_n v_n + q_e n_p v_p$ ($\mathrm{A\ m^{-2}}$); conductivity $\sigma = q_e n_e \mu_e + q_e n_n \mu_i + q_e n_p \mu_i$ ($\mathrm{S\ m^{-1}}$); current $I(z,t) = d^2 J(z,t)$ (A); current moment $IL(t) = \int_0^d I(z,t)dz$ (A m); dipole moment $QL = \int_0^\infty IL(t)dt$ (C m); second positive band system of N_2 emission intensity $I_{sp}(t) = \frac{d^2 A_{sp}}{A_{sp} + k_q n_{O2}} \int_0^d \nu_{sp} n_e dz$ (photons $\mathrm{s^{-1}}$); and the total number of photons of the second positive band system of N_2 $N_{sp} = \int_0^\infty I_{sp}(t)dt$. The fast breakdown velocity $v_{fb}(t)$ (m/s) is calculated by monitoring the time-dependent position of $\max(n_e E)$. The reported modeling does not resolve spatial distributions and dynamics of charge and current densities associated with the negative charge accumulating at $z = 0$, and the reported $v_{fb}(t)$ (m/s) therefore represents the fast positive breakdown velocity following terminology adopted in existing literature (Rison et al., 2016; Tilles et al., 2019).

Data Availability Statement

The original data presented in this paper as figures may be downloaded from https://doi.org/10.26208/9NJA-G306 (Pasko et al., 2025).

Acknowledgments
This research has been supported by the Aeronomy Program of the National Science Foundation under Grants AGS-2329677 and AGS-2341623 to Penn State University. S. Celestin acknowledges support from the French space agency (CNES) within the projects OREO and STRATELEC, by the French Region Centre-Val-de-Loire, and by the Institut Universitaire de France (IUF). J. Jansky gratefully acknowledges financial support from the Grant VAROPS (DZRO FVT 3) granted by the Ministry of Defense of the Czech Republic.

References

Abbasi, R. U., Abu-Zayyad, T., Allen, M., Barcikowski, E., Belz, J. W., Bergman, D. R., et al. (2018). Gamma ray showers observed at ground level in coincidence with downward lightning leaders. *Journal of Geophysical Research*, *123*(13), 6864–6879. https://doi.org/10.1029/2017JD027931

Abbasi, R. U., Kieu, N., Krehbiel, P. R., Belz, J. W., Saba, M. M. F., Rison, W., et al. (2024). Intermediate fluence downward terrestrial gamma ray flashes as observed by the Telescope Array Surface Detector. *Journal of Geophysical Research*, *129*(24), e2024JD041260. https://doi.org/10.1029/2024JD041260

Abbasi, R. U., Saba, M. M. F., Belz, J. W., Krehbiel, P. R., Rison, W., Kieu, N., et al. (2023). First high-speed video camera observations of a lightning flash associated with a downward terrestrial gamma-ray flash. *Geophysical Research Letters*, *50*(14), e2023GL102958. https://doi.org/10.1029/2023GL102958

Alnussirat, S. T., Cherry, M. L., Christian, H. J., & Burchfield, J. C. (2023). Simultaneous space-based observations of TGFs and lightning optical emission: Characteristics of lightning. *Journal of Geophysical Research*, *128*(1), e2022JA030364. https://doi.org/10.1029/2022JA030364

Arabshahi, S., Dwyer, J. R., Nag, A., Rakov, V. A., & Rassoul, H. K. (2014). Numerical simulations of compact intracloud discharges as the relativistic runaway electron avalanche-extensive air shower process. *Journal of Geophysical Research*, *119*(1), 479–489. https://doi.org/10.1002/2013JA018974

Babich, L. P., & Bochkov, E. I. (2011). Deterministic methods for numerical simulation of high-energy runaway electron avalanches. *Journal of Experimental and Theoretical Physics (Translation of Zhurnal Eksperimental'noi i Teoreticheskoi Fiziki)*, *112*(3), 494–503. https://doi.org/10.1134/S1063776111020014

Belz, J. W., Krehbiel, P. R., Remington, J., Stanley, M. A., Abbasi, R. U., LeVon, R., et al. (2020). Observations of the origin of downward terrestrial gamma-ray flashes. *Journal of Geophysical Research*, *125*(23), e2019JD031940. https://doi.org/10.1029/2019JD031940

Berge, N., & Celestin, S. (2019). Constraining downward terrestrial gamma ray flashes using ground-based particle detector arrays. *Geophysical Research Letters*, *46*(14), 8424–8430. https://doi.org/10.1029/2019GL083252

Bjorge-Engeland, I. (2024). *The connection between lightning currents, TGF intensities and Elves*. Ph.D. Thesis. University of Bergen, Bergen 5020, Norway.

Bjorge-Engeland, I., Ostgaard, N., Mezentsev, A., Skeie, C. A., Sarria, D., Lapierre, J., et al. (2022). Terrestrial gamma-ray flashes with accompanying elves detected by ASIM. *Journal of Geophysical Research*, *127*(11), e2021JD036368. https://doi.org/10.1029/2021JD036368

Bjorge-Engeland, I., Ostgaard, N., Sarria, D., Marisaldi, M., Mezentsev, A., Fuglestad, A., et al. (2024). Evidence of a new population of weak terrestrial gamma-ray flashes observed from aircraft altitude. *Geophysical Research Letters*, *51*(17), e2024GL110395. https://doi.org/10.1029/2024GL110395

Boeuf, J. P. (2003). Plasma display panels: Physics, recent developments and key issues. *Journal of Physics D Applied Physics*, *36*(6), R53–R79. https://doi.org/10.1088/0022-3727/36/6/201

Bourdon, A., Pasko, V. P., Liu, N. Y., Celestin, S., Segur, P., & Marode, E. (2007). Efficient models for photoionization produced by non-thermal gas discharges in air based on radiative transfer and the Helmholtz equations. *Plasma Sources Science and Technology*, *16*(3), 656–678. https://doi.org/10.1088/0963-0252/16/3/026

Briggs, M. S., Connaughton, V., Wilson-Hodge, C., Preece, R. D., Fishman, G. J., Kippen, R. M., et al. (2011). Electron-positron beams from terrestrial lightning observed with Fermi GBM. *Geophysical Research Letters*, *38*(2), L02808. https://doi.org/10.1029/2010GL046259

Carlson, B. E., Lehtinen, N. G., & Inan, U. S. (2010). Neutron production in terrestrial gamma ray flashes. *Journal of Geophysical Research*, *115*(A4), A00E19. https://doi.org/10.1029/2009JA014696

Celestin, S., & Pasko, V. P. (2011). Energy and fluxes of thermal runaway electrons produced by exponential growth of streamers during the stepping of lightning leaders and in transient luminous events. *Journal of Geophysical Research*, *116*(A3), A03315. https://doi.org/10.1029/2010ja016260

Celestin, S., Xu, W., & Pasko, V. P. (2015). Variability in fluence and spectrum of high-energy photon bursts produced by lightning leaders. *Journal of Geophysical Research*, *120*(12), 10712–10723. https://doi.org/10.1002/2015JA021410

Chaffin, J. M., Smith, D. M., Lapierre, J., Cummer, S., Ortberg, J., Sunjerga, A., et al. (2024). Mountaintop gamma ray observations of three terrestrial gamma-ray flashes at the Säntis Tower, Switzerland with coincident radio waveforms. *Journal of Geophysical Research*, *129*(2), e2023JD039761. https://doi.org/10.1029/2023JD039761

Chanrion, O., Neubert, T., Mogensen, A., Yair, Y., Stendel, M., Singh, R., & Siingh, D. (2017). Profuse activity of blue electrical discharges at the tops of thunderstorms. *Geophysical Research Letters*, *44*(1), 496–503. https://doi.org/10.1002/2016GL071311

Chapman, R., Marshall, T., Karunarathne, S., & Stolzenburg, M. (2017). Initial electric field changes of lightning flashes in two thunderstorms. *Journal of Geophysical Research*, *122*(7), 3718–3732. https://doi.org/10.1002/2016JD025859

Chen, S., Rakov, V. A., Zhu, Y., & Ding, Z. (2024). Clusters of compact intracloud discharges (CIDs) in overshooting convective surges. *Journal of Geophysical Research*, *129*(8), e2023JD040307. https://doi.org/10.1029/2023JD040307

Chou, J.-K., Hsu, R.-R., Su, H.-T., Chen, A. B.-C., Kuo, C.-L., Huang, S.-M., et al. (2018). ISUAL-observed blue luminous events: The associated sferics. *Journal of Geophysical Research*, *123*(4), 3063–3077. https://doi.org/10.1002/2017JA024793

Coleman, L. M., & Dwyer, J. R. (2006). Propagation speed of runaway electron avalanches. *Geophysical Research Letters*, *33*(11), L11810. https://doi.org/10.1029/2006GL025863

Cummer, S. A. (2020). Indirectly measured ambient electric fields for lightning initiation in fast breakdown regions. *Geophysical Research Letters*, *47*(4), e2019GL086089. https://doi.org/10.1029/2019GL086089

da Silva, C. L., & Pasko, V. P. (2013). Dynamics of streamer-to-leader transition at reduced air densities and its implications for propagation of lightning leaders and gigantic jets. *Journal of Geophysical Research*, *118*(24), 13561–13590. https://doi.org/10.1002/2013jd020618

da Silva, C. L., & Pasko, V. P. (2015). Physical mechanism of initial breakdown pulses and narrow bipolar events in lightning discharges. *Journal of Geophysical Research*, *120*(10), 4989–5009. https://doi.org/10.1002/2015JD023209

Dwyer, J. R. (2003). A fundamental limit on electric fields in air. *Geophysical Research Letters*, *30*(20), 2055. https://doi.org/10.1029/2003GL017781

Dwyer, J. R. (2007). Relativistic breakdown in planetary atmospheres. *Physics of Plasmas*, *14*(4), 042901. https://doi.org/10.1063/1.2709652

Dwyer, J. R. (2012). The relativistic feedback discharge model of terrestrial gamma ray flashes. *Journal of Geophysical Research*, *117*(A2), A02308. https://doi.org/10.1029/2011JA017160
Dwyer, J. R. (2025). Energetic particles produced by thunderstorm electric fields. *Journal of Geophysical Research*, *130*(2), e2024JD042193. https://doi.org/10.1029/2024JD042193
Dwyer, J. R., & Babich, L. P. (2011). Low-energy electron production by relativistic runaway electron avalanches in air. *Journal of Geophysical Research*, *116*(A9), A09301. https://doi.org/10.1029/2011JA016494
Dwyer, J. R., Liu, N., & Rassoul, H. K. (2013). Properties of the thundercloud discharges responsible for terrestrial gamma-ray flashes. *Geophysical Research Letters*, *40*(15), 4067–4073. https://doi.org/10.1002/grl.50742
Dwyer, J. R., Rassoul, H. K., Al-Dayeh, M., Caraway, L., Chrest, A., Wright, B., et al. (2005). X-ray bursts associated with leader steps in cloud-to-ground lightning. *Geophysical Research Letters*, *32*(1), L01803. https://doi.org/10.1029/2004GL021782
Dwyer, J. R., Smith, D. M., & Cummer, S. A. (2012). High-energy atmospheric physics: Terrestrial gamma-ray flashes and related phenomena. *Space Science Reviews*, *173*(1–4), 133–196. https://doi.org/10.1007/s11214-012-9894-0
Dwyer, J. R., & Uman, M. A. (2014). The physics of lightning. *Physics Reports*, *534*(4), 147–241. https://doi.org/10.1016/j.physrep.2013.09.004
Eack, K. B., & Beasley, W. H. (2015). Long-duration X-ray emissions observed in thunderstorms. *Journal of Geophysical Research*, *120*(14), 6887–6897. https://doi.org/10.1002/2015JD023262
Eack, K. B., Beasley, W. H., Rust, W. D., Marshall, T. C., & Stolzenburg, M. (1996). X-ray pulses observed above a mesoscale convective system. *Geophysical Research Letters*, *23*(21), 2915–2918. https://doi.org/10.1029/96GL02570
Fishman, G. J., Bhat, P. N., Mallozzi, R., Horack, J. M., Koshut, T., Kouveliotou, C., et al. (1994). Discovery of intense gamma-ray flashes of atmospheric origin. *Science*, *264*(5163), 1313–1316. https://doi.org/10.1126/science.264.5163.1313
Gourbin, P., & Celestin, S. (2024a). On the self-quenching of relativistic runaway electron avalanches producing terrestrial gamma ray flashes. *Geophysical Research Letters*, *51*(10), e2023GL107488. https://doi.org/10.1029/2023GL107488
Gourbin, P., & Celestin, S. (2024b). Self consistent modeling of relativistic runaway electron beams giving rise to terrestrial gamma-rays flashes. *Journal of Geophysical Research*, *129*(5), e2023JA032278. https://doi.org/10.1029/2023JA032278
Gurevich, A., Zybin, K., & Medvedev, Y. (2006). Amplification and nonlinear modification of runaway breakdown. *Physics Letters A*, *349*(5), 331–339. https://doi.org/10.1016/j.physleta.2005.09.074
Hagelaar, G., & Pitchford, L. (2005). Solving the Boltzmann equation to obtain electron transport coefficients and rate coefficients for fluid models. *Plasma Sources Science and Technology*, *14*(4), 722–733. https://doi.org/10.1088/0963-0252/14/4/011
Heumesser, M., Chanrion, O., Neubert, T., Christian, H. J., Dimitriadou, K., Gordillo-Vazquez, F. J., et al. (2021). Spectral observations of optical emissions associated with terrestrial gamma-ray flashes. *Geophysical Research Letters*, *48*(4), e2020GL090700. https://doi.org/10.1029/2020GL090700
Huang, A., Cummer, S. A., & Pu, Y. (2021). Lightning initiation from fast negative breakdown is led by positive polarity dominated streamers. *Geophysical Research Letters*, *48*(8), e2020GL091553. https://doi.org/10.1029/2020GL091553
Jacobson, A. R., Light, T. E. L., Hamlin, T., & Nemzek, R. (2013). Joint radio and optical observations of the most radio-powerful intracloud lightning discharges. *Annals of Geophysics*, *31*(3), 563–580. https://doi.org/10.5194/angeo-31-563-2013
Janalizadeh, R., & Pasko, V. P. (2019). A general framework for photoionization calculations applied to nonthermal gas discharges in air. *Plasma Sources Science and Technology*, *28*(10), 105006. https://doi.org/10.1088/1361-6595/ab4374
Janalizadeh, R., & Pasko, V. P. (2020). A framework for efficient calculation of photoionization and photodetachment rates with application to the lower ionosphere. *Journal of Geophysical Research*, *128*(7), e2020JA027979. https://doi.org/10.1029/2020JA027979
Janalizadeh, R., & Pasko, V. P. (2021). Implications of electron detachment in associative collisions of atomic oxygen anion with molecular nitrogen for modeling of transient luminous events. *Geophysical Research Letters*, *48*(4), e2020GL091. https://doi.org/10.1029/2020gl091134
Jansky, J., Janalizadeh, R., & Pasko, V. P. (2025). Investigation of ignition of positive corona discharge in air using a time dependent fluid model. *Plasma Sources Science and Technology*, *34*(2), 025014. https://doi.org/10.1088/1361-6595/adb518
Jansky, J., & Pasko, V. P. (2020). Modeling of streamer ignition and propagation in the system of two approaching hydrometeors. *Journal of Geophysical Research*, *125*(6), e2019JD031337. https://doi.org/10.1029/2019JD031337
Karunarathne, N., Karunarathne, S., Marshall, T. C., & Stolzenburg, M. (2019). Modeling initial breakdown pulses of lightning flashes using a matrix inversion method. *Radio Science*, *54*(3), 268–280. https://doi.org/10.1029/2018rs006695
Karunarathne, N., Marshall, T. C., Karunarathne, S., & Stolzenburg, M. (2021). Modeling initial breakdown pulses of intracloud lightning flashes. *Atmospheric Research*, *261*, 105734. https://doi.org/10.1016/j.atmosres.2021.105734
Kieu, N., Abbasi, R. U., Saba, M. M. F., Belz, J. W., Krehbiel, P. R., Stanley, M. A., et al. (2024). First time-resolved leader spectra associated with a downward terrestrial gamma-ray flash detected at the telescope array surface detector. *Journal of Geophysical Research*, *129*(24), e2024JD041720. https://doi.org/10.1029/2024JD041720
Kirkland, M., Suszcynsky, D., Guillen, J., & Green, J. (2001). Optical observations of terrestrial lightning by the FORTE satellite photodiode detector. *Journal of Geophysical Research*, *106*(D24), 33499–33509. https://doi.org/10.1029/2000JD000190
Kohn, C., Heumesser, M., Chanrion, O., Nishikawa, K., Reglero, V., & Neubert, T. (2020). The emission of terrestrial gamma ray flashes from encountering streamer coronae associated to the breakdown of lightning leaders. *Geophysical Research Letters*, *47*(20), e2020GL089749. https://doi.org/10.1029/2020GL089749
Kossyi, I. A., Kostinsky, A. Y., Matveyev, A. A., & Silakov, V. P. (1992). Kinetic scheme of the non-equilibrium discharge in nitrogen-oxygen mixtures. *Plasma Sources Science and Technology*, *1*(3), 207–220. https://doi.org/10.1088/0963-0252/1/3/011
Kostinskiy, A. Y., Marshall, T. C., & Stolzenburg, M. (2020). The mechanism of the origin and development of lightning from initiating event to initial breakdown pulses (v.2). *Journal of Geophysical Research*, *125*(22), e2020JD033191. https://doi.org/10.1029/2020JD033191
Li, D., Neubert, T., Husbjerg, L. S., Zhu, Y., Chanrion, O., Lapierre, J., et al. (2023). Observation of blue corona discharges and cloud microphysics in the top of thunderstorm cells in cyclone Fani. *Journal of Geophysical Research*, *128*(21), e2022JD038328. https://doi.org/10.1029/2022JD038328
Lindanger, A., Marisaldi, M., Sarria, D., Ostgaard, N., Lehtinen, N., Skeie, C. A., et al. (2021). Spectral analysis of individual terrestrial gamma-ray flashes detected by ASIM. *Journal of Geophysical Research*, *126*(23), e2021JD035347. https://doi.org/10.1029/2021JD035347
Liu, F., Neubert, T., Chanrion, O., Lu, G., Wu, T., Lyu, F., et al. (2024). Polarity transitions of narrow bipolar events in thundercloud tops reaching the lower stratosphere. *Nature Communications*, *15*(1), 7344. https://doi.org/10.1038/s41467-024-51705-y
Liu, F., Zhu, B., Lu, G., Qin, Z., Lei, J., Peng, K.-M., et al. (2018). Observations of blue discharges associated with negative narrow bipolar events in active deep convection. *Geophysical Research Letters*, *45*(6), 2842–2851. https://doi.org/10.1002/2017GL076207
Liu, L., & Becerra, M. (2017). An efficient model to simulate stable glow corona discharges and their transition into streamers. *Journal of Physics D Applied Physics*, *50*(10), 105204. https://doi.org/10.1088/1361-6463/aa5a34

Liu, N., Dwyer, J. R., Tilles, J. N., Stanley, M. A., Krehbiel, P. R., Rison, W., et al. (2019). Understanding the radio spectrum of thunderstorm narrow bipolar events. *Journal of Geophysical Research*, *124*(17–18), 10134–10153. https://doi.org/10.1029/2019JD030439

Liu, N. Y., & Dwyer, J. R. (2013). Modeling terrestrial gamma ray flashes produced by relativistic feedback discharges. *Journal of Geophysical Research*, *118*(5), 2359–2376. https://doi.org/10.1002/jgra.50232

Liu, N. Y., & Pasko, V. P. (2004). Effects of photoionization on propagation and branching of positive and negative streamers in sprites. *Journal of Geophysical Research*, *109*(A4), A04301. https://doi.org/10.1029/2003JA010064

Liu, N. Y., Scholten, O., Hare, B. M., Dwyer, J. R., Sterpka, C. F., Kolmasova, I., & Santolik, O. (2022). LOFAR observations of lightning initial breakdown pulses. *Geophysical Research Letters*, *49*(6), e2022GL098073. https://doi.org/10.1029/2022GL098073

Lu, G., Blakeslee, R. J., Li, J., Smith, D. M., Shao, X. M., McCaul, E. W., et al. (2010). Lightning mapping observation of a terrestrial gamma-ray flash. *Geophysical Research Letters*, *37*(11), L11806. https://doi.org/10.1029/2010GL043494

Lyu, F., Cummer, S. A., Briggs, M., Marisaldi, M., Blakeslee, R. J., Bruning, E., et al. (2016). Ground detection of terrestrial gamma ray flashes from distant radio signals. *Geophysical Research Letters*, *43*(16), 8728–8734. https://doi.org/10.1002/2016GL070154

Lyu, F., Cummer, S. A., & McTague, L. (2015). Insights into high peak current in-cloud lightning events during thunderstorms. *Geophysical Research Letters*, *42*(16), 6836–6843. https://doi.org/10.1002/2015GL065047

Lyu, F., Cummer, S. A., Qin, Z., & Chen, M. (2019). Lightning initiation processes imaged with very high frequency broadband interferometry. *Journal of Geophysical Research*, *124*(6), 2994–3004. https://doi.org/10.1029/2018JD029817

Lyu, F., Qin, Z., Cummer, S. A., Zheng, Y., Jiang, S., Zheng, T., et al. (2024). Source altitude of energetic in-cloud pulses inside thunderstorms and implication for the intrinsic brightness of terrestrial gamma-ray flashes. *Geophysical Research Letters*, *51*(20), e2024GL110598. https://doi.org/10.1029/2024GL110598

Marisaldi, M., Fuschino, F., Labanti, C., Galli, M., Longo, F., Del Monte, E., et al. (2010). Detection of terrestrial gamma ray flashes up to 40 MeV by the AGILE satellite. *Journal of Geophysical Research*, *115*(A3), A00E13. https://doi.org/10.1029/2009JA014502

Marisaldi, M., Ostgaard, N., Mezentsev, A., Lang, T., Grove, J. E., Shy, D., et al. (2024). Highly dynamic gamma-ray emissions are common in tropical thunderclouds. *Nature*, *634*(8032), 57–60. https://doi.org/10.1038/s41586-024-07936-6

Marshall, T., Bandara, S., Karunarathne, N., Karunarathne, S., Kolmasova, I., Siedlecki, R., & Stolzenburg, M. (2019). A study of lightning flash initiation prior to the first initial breakdown pulse. *Atmospheric Research*, *217*, 10–23. https://doi.org/10.1016/j.atmosres.2018.10.013

Marshall, T., Stolzenburg, M., Karunarathna, N., & Karunarathne, S. (2014). Electromagnetic activity before initial breakdown pulses of lightning. *Journal of Geophysical Research*, *119*(22), 12558–12574. https://doi.org/10.1002/2014JD022155

Marshall, T., Stolzenburg, M., Karunarathne, S., Cummer, S., Lu, G., Betz, H.-D., et al. (2013). Initial breakdown pulses in intracloud lightning flashes and their relation to terrestrial gamma ray flashes. *Journal of Geophysical Research*, *118*(19), 10907–10925. https://doi.org/10.1002/jgrd.50866

Marshall, T. C., McCarthy, M. P., & Rust, W. D. (1995). Electric field magnitudes and lightning initiation in thunderstorms. *Journal of Geophysical Research*, *100*(D4), 7097–7104. https://doi.org/10.1029/95JD00020

McCarthy, M. P., & Parks, G. K. (1992). On the modulation of X-ray fluxes in thunderstorms. *Journal of Geophysical Research*, *97*(D5), 5857–5864. https://doi.org/10.1029/91jd03160

McHarg, M. G., Harley, J. L., Ashcraft, T., & Stenbaek-Nielsen, H. C. (2021). Sprite lightning at 100,000 frames per second. *Astronomy Picture of the Day*. https://apod.nasa.gov/apod/ap210104.html

Mezentsev, A., Ostgaard, N., Marisaldi, M., Sarria, D., Lehtinen, N., Neubert, T., et al. (2024). Discerning TGF and leader current pulse in ASIM observation. *Geophysical Research Letters*, *51*(22), e2024GL110554. https://doi.org/10.1029/2024GL110554

Moore, C. B., Eack, K. B., Aulich, G. D., & Rison, W. (2001). Energetic radiation associated with lightning stepped-leaders. *Geophysical Research Letters*, *28*(11), 2141–2144. https://doi.org/10.1029/2001GL013140

Moss, G. D., Pasko, V. P., Liu, N. Y., & Veronis, G. (2006). Monte Carlo model for analysis of thermal runaway electrons in streamer tips in transient luminous events and streamer zones of lightning leaders. *Journal of Geophysical Research*, *111*(A2), A02307. https://doi.org/10.1029/2005JA011350

Nag, A., & Rakov, V. A. (2010). Compact intracloud lightning discharges: 2. Estimation of electrical parameters. *Journal of Geophysical Research*, *115*(D20), D20103. https://doi.org/10.1029/2010JD014237

Nag, A., Rakov, V. A., Tsalikis, D., & Cramer, J. A. (2010). On phenomenology of compact intracloud lightning discharges. *Journal of Geophysical Research*, *115*(D14), D14115. https://doi.org/10.1029/2009JD012957

Naidis, G. V. (2005). Conditions for inception of positive corona discharges in air. *Journal of Physics D Applied Physics*, *38*(13), 2211–2214. https://doi.org/10.1088/0022-3727/38/13/020

Neubert, T., Chanrion, O., Heumesser, M., Dimitriadou, K., Husbjerg, L., Rasmussen, I. L., et al. (2021). Observation of the onset of a blue jet into the stratosphere. *Nature*, *589*(7842), 371–375. https://doi.org/10.1038/s41586-020-03122-6

Neubert, T., Ostgaard, N., Reglero, V., Chanrion, O., Heumesser, M., Dimitriadou, K., et al. (2020). A terrestrial gamma-ray flash and ionospheric ultraviolet emissions powered by lightning. *Science*, *367*(6474), 183–186. https://doi.org/10.1126/science.aax3872

Ostgaard, N., Cummer, S. A., Mezentsev, A., Luque, A., Dwyer, J., Neubert, T., et al. (2021). Simultaneous observations of EIP, TGF, ELVE, and optical lightning. *Journal of Geophysical Research*, *126*(11), e2020JD033921. https://doi.org/10.1029/2020JD033921

Ostgaard, N., Mezentsev, A., Marisaldi, M., Grove, J. E., Quick, M., Christian, H., et al. (2024). Flickering gamma-ray flashes, the missing link between gamma glows and TGFS. *Nature*, *634*(8032), 53–56. https://doi.org/10.1038/s41586-024-07893-0

Parks, G., Mauk, B., Spiger, R., & Chin, J. (1981). X-ray enhancements detected during thunderstorm and lightning activities. *Geophysical Research Letters*, *8*(11), 1176–1179. https://doi.org/10.1029/GL008i011p01176

Pasko, V. P. (2006). Theoretical modeling of sprites and jets, in sprites, elves and intense lightning discharges. In M. Füllekrug, E. A. Mareev, & M. J. Rycroft (Eds.), *NATO science series II: Mathematics, physics and chemistry* (Vol. 225, pp. 253–311). Springer.

Pasko, V. P. (2014). Electrostatic modeling of intra-cloud stepped leader electric fields and mechanisms of terrestrial gamma ray flashes. *Geophysical Research Letters*, *41*(1), 179–185. https://doi.org/10.1002/2013GL058983

Pasko, V. P., Celestin, S., & Bourdon, A. (2024). Photoelectric feedback mechanism for acceleration of runaway electrons in gas discharges at high overvoltages. *Physical Review Letters*, *133*(23), 235301. https://doi.org/10.1103/PhysRevLett.133.235301

Pasko, V. P., Celestin, S., Bourdon, A., Janalizadeh, R., & Jansky, J. (2023). Conditions for inception of relativistic runaway discharges in air. *Geophysical Research Letters*, *50*(7), e2022GL102710. https://doi.org/10.1029/2022GL102710

Pasko, V. P., Celestin, S., Bourdon, A., Janalizadeh, R., Pervez, Z., Jansky, J., & Gourbin, P. (2025). Photoelectric effect in air explains lightning initiation and terrestrial gamma ray flashes [Dataset]. *Penn State Data Commons*. https://doi.org/10.26208/9NJA-G306

Pasko, V. P., Inan, U. S., Bell, T. F., & Reising, S. C. (1998). Mechanism of ELF radiation from sprites. *Geophysical Research Letters*, *25*(18), 3493–3496. https://doi.org/10.1029/98gl02631

Pasko, V. P., Janalizadeh, R., & Jansky, J. (2023). Investigation of conditions necessary for inception of positive corona in air based on differential formulation of photoionization. *Plasma Sources Science and Technology*, *32*(7), 075014. https://doi.org/10.1088/1361-6595/ace6d0

Pervez, Z., Janalizadeh, R., & Pasko, V. P. (2024a). Remote sensing of source currents of narrow bipolar events using measured electric fields. *Geophysical Research Letters*, *51*(7), e2023GL107789. https://doi.org/10.1029/2023GL107789

Pervez, Z., Janalizadeh, R., & Pasko, V. P. (2024b). Compact intracloud discharges and the sources generating their low and high frequency signatures. In *Abstract AE11B-2660 presented at 2024 fall meeting, AGU, Washington, DC, 9-10 December 2024*.

Pu, Y., & Cummer, S. A. (2024). Imaging step formation in in-cloud lightning initial development with VHF interferometry. *Geophysical Research Letters*, *51*(1), e2023GL107388. https://doi.org/10.1029/2023GL107388

Pu, Y., Cummer, S. A., Huang, A., Briggs, M., Mailyan, B., & Lesage, S. (2020). A satellite-detected terrestrial gamma ray flash produced by a cloud-to-ground lightning leader. *Geophysical Research Letters*, *47*(15), e2020GL089427. https://doi.org/10.1029/2020GL089427

Pu, Y., Cummer, S. A., Lyu, F., Briggs, M., Mailyan, B., Stanbro, M., & Roberts, O. (2019). Low frequency radio pulses produced by terrestrial gamma-ray flashes. *Geophysical Research Letters*, *46*(12), 6990–6997. https://doi.org/10.1029/2019GL082743

Rison, W., Krehbiel, P. R., Stock, M. G., Edens, H. E., Shao, X.-M., Thomas, R. J., et al. (2016). Observations of narrow bipolar events reveal how lightning is initiated in thunderstorms. *Nature Communications*, *7*(1), 10721. https://doi.org/10.1038/ncomms10721

Shao, X.-M., Hamlin, T., & Smith, D. M. (2010). A closer examination of terrestrial gamma-ray flash-related lightning processes. *Journal of Geophysical Research*, *115*(A6), A00E30. https://doi.org/10.1029/2009JA014835

Shao, X.-M., Jensen, D. P., Ho, C., Caffrey, M. P., Raby, E. Y., Graham, P. S., et al. (2025). 3D radio frequency mapping and polarization observations show lightning flashes were ignited by cosmic-ray showers. *Journal of Geophysical Research*, *130*(5), e2024JD042549. https://doi.org/10.1029/2024JD042549

Skeie, C. A., Ostgaard, N., Mezentsev, A., Bjorge-Engeland, I., Marisaldi, M., Lehtinen, N., et al. (2022). The temporal relationship between terrestrial gamma-ray flashes and associated optical pulses from lightning. *Journal of Geophysical Research*, *127*(17), e2022JD037128. https://doi.org/10.1029/2022JD037128

Smith, D., Eack, K., Harlin, J., Heavner, M., Jacobson, A., Massey, R., et al. (2002). The Los Alamos Sferic array: A research tool for lightning investigations. *Journal of Geophysical Research*, *107*(D13), 4183. https://doi.org/10.1029/2001JD000502

Smith, D. M., Lopez, L. I., Lin, R. P., & Barrington-Leigh, C. P. (2005). Terrestrial gamma-ray flashes observed up to 20 MeV. *Science*, *307*(5712), 1085–1088. https://doi.org/10.1126/science.1107466

Soler, S., Gordillo-Vazquez, F. J., Perez-Invernon, F. J., Luque, A., Li, D., Neubert, T., et al. (2021). Global frequency and geographical distribution of nighttime streamer corona discharges (BLUEs) in thunderclouds. *Geophysical Research Letters*, *48*(18), e2021GL094657. https://doi.org/10.1029/2021GL094657

Stanley, M., Shao, X., Smith, D., Lopez, L., Pongratz, M., Harlin, J., et al. (2006). A link between terrestrial gamma-ray flashes and intracloud lightning discharges. *Geophysical Research Letters*, *33*(6), L06803. https://doi.org/10.1029/2005GL025537

Stenbaek-Nielsen, H. C., Mcharg, M. G., & Liu, N. Y. (2025). Observed sprite streamer growth rates. *Geophysical Research Letters*, *52*(1), e2024GL112537. https://doi.org/10.1029/2024GL112537

Stolzenburg, M., Marshall, T. C., Karunarathne, S., Karunarathna, N., & Orville, R. E. (2014). Leader observations during the initial breakdown stage of a lightning flash. *Journal of Geophysical Research*, *119*(21), 12198–12221. https://doi.org/10.1002/2014JD021994

Stolzenburg, M., Marshall, T. C., Karunarathne, S., Karunarathna, N., Vickers, L. E., Warner, T. A., et al. (2013). Luminosity of initial breakdown in lightning. *Journal of Geophysical Research*, *118*(7), 2918–2937. https://doi.org/10.1002/jgrd.50276

Stolzenburg, M., Marshall, T. C., Karunarathne, S., & Orville, R. E. (2016). Luminosity with intracloud-type lightning initial breakdown pulses and terrestrial gamma-ray flash candidates. *Journal of Geophysical Research*, *121*(18), 10919–10936. https://doi.org/10.1002/2016JD025202

Stolzenburg, M., Marshall, T. C., Rust, W. D., Bruning, E., MacGorman, D. R., & Hamlin, T. (2007). Electric field values observed near lightning flash initiations. *Geophysical Research Letters*, *34*(4), L04804. https://doi.org/10.1029/2006GL028777

Suszcynsky, D. M., Roussel-Dupre, R., & Shaw, G. (1996). Ground-based search for X rays generated by thunderstorms and lightning. *Journal of Geophysical Research*, *101*(D18), 23505–23516. https://doi.org/10.1029/96JD02134

Tilles, J. N., Krehbiel, P. R., Stanley, M. A., Rison, W., Liu, N., Lyu, F., et al. (2020). Radio interferometer observations of an energetic in-cloud pulse reveal large currents generated by relativistic discharges. *Journal of Geophysical Research*, *125*(20), e2020JD032603. https://doi.org/10.1029/2020JD032603

Tilles, J. N., Liu, N., Stanley, M. A., Krehbiel, P. R., Rison, W., Stock, M. G., et al. (2019). Fast negative breakdown in thunderstorms. *Nature Communications*, *10*(1), 1648. https://doi.org/10.1038/s41467-019-09621-z

Tsuchiya, H., Enoto, T., Iwata, K., Yamada, S., Yuasa, T., Kitaguchi, T., et al. (2013). Hardening and termination of long-duration γ rays detected prior to lightning. *Physical Review Letters*, *111*(1), 015001. https://doi.org/10.1103/PhysRevLett.111.015001

Ueda, S., Hasegawa, M., Baba, Y., & Rakov, V. A. (2024). Wave guiding properties of large low-conductivity cylinders. *IEEE Transactions on Electromagnetic Compatibility*, *66*(4), 1183–1191. https://doi.org/10.1109/TEMC.2024.3408849

Wada, Y., Matsumoto, T., Enoto, T., Nakazawa, K., Yuasa, T., Furuta, Y., et al. (2021). Catalog of gamma-ray glows during four winter seasons in Japan. *Physical Review Research*, *3*(4), 043117. https://doi.org/10.1103/PhysRevResearch.3.043117

Williams, E., Boldi, R., Bor, J., Satori, G., Price, C., Greenberg, E., et al. (2006). Lightning flashes conducive to the production and escape of gamma radiation to space. *Journal of Geophysical Research*, *111*(D16), D16209. https://doi.org/10.1029/2005JD006447

Xu, W., Celestin, S., & Pasko, V. P. (2015). Optical emissions associated with terrestrial gamma ray flashes. *Journal of Geophysical Research*, *120*(2), 1355–1370. https://doi.org/10.1002/2014JA020425

Zhang, H., Lu, G., Lyu, F., Xiong, S., Ahmad, M. R., Yi, Q., et al. (2021). On the terrestrial gamma-ray flashes preceding narrow bipolar events. *Geophysical Research Letters*, *48*(8), e2020GL092160. https://doi.org/10.1029/2020GL092160